Front. Phys., 2013, 8(1): 1–19
DOI 10.1007/s11467-013-0280-5

REVIEW ARTICLE

Optical properties of one-dimensional soft photonic crystals with ferrofluids

Chun-Zhen Fan[1,2,*], **Er-Jun Liang**[1,†], **Ji-Ping Huang**[2,‡]

[1] *School of Physical Science and Engineering, and Key Laboratory of Materials Physics of Ministry of Education of China, Zhengzhou University, Zhengzhou 450052, China*

[2] *State Key Laboratory of Surface Physics and Department of Physics, Fudan University, Shanghai 200433, China*

E-mail: * *chunzhen@zzu.edu.cn*, † *ejliang@zzu.edu.cn*, ‡ *jphuang@fudan.edu.cn*

Received December 17, 2012; accepted December 26, 2012

We review the recent theoretical study on the optical properties of one-dimensional soft photonic crystals (1D SPCs) with ferrofluids. The proposed structure is composed of alternating ferrofluid layers and dielectric layers. For the ferrofluid, single domain ferromagnetic nanoparticles can align to a chain under the stimuli of an external magnetic field, thus changing the microstructure of the system. Meanwhile, nonlinear optical responses in ferrofluids are also briefly reviewed.

Keywords soft photonic crystals, ferrofluids, band gap

PACS numbers 42.70.Qs, 47.65.Cb

Contents

1 Introduction

Photonic crystals (PCs) are periodic arrays of material with different refractive index [1, 2]. It was first put forth independently by Yablonovitch and John in 1987 [3, 4]. The major functionality of the PCs is the strong distortion or modification of dispersion, which can influence the behavior of photons. PCs have attracted a wide research attentions owing to their unique light manipulation abilities, demonstrating wide applications in optical sensor, optical filter and various optical integrated circuit devices [5–7]. They are usually composed of the solid material like silicon [8, 9], which can be realized through the combination with semiconductor material to form the Si-SiO_2, SiO_2-GaAs or Si-AlGaAs structure by the dry ethching method or the wet electrochemical process [10]. However, it is an alternative to fabricate PCs with colloidal suspension like the soft photonic crystals (SPCs) at a low cost and fast response, which can be realized through the self-assembled colloidal microspheres or tuned with different external stimuli [11–13]. Until now, much work has been carried out to study the SPCs, like the dually tunable SPCs composed of thermosensitive gel particles [14], soft glass photonic crystal fibers [15], and the hydrogel colloidal crystals achieved

by simply varying the water content of the microgel pellet before annealing and crystallization [16]. In this work, we review our recent theoretical study in SPCs, which is composed of alternating ferrofluid layers and dielectric layers.

In general, ferrofluids is a type of colloidal suspension, in which single domain ferromagnetic nanoparticles (about 10 nm in diameter) randomly disperse in polar or nonpolar liquid [17–26]. Typically, ferrofluids consists of ferromagnetic particles (like Co or Fe_3O_4) or ferrimagnetic nanoparticles (like $CoFe_2O_4$) [27], coated with surfactant to prevent their aggregation due to the van der Waals and magnetic forces [27–30]. This stable suspension would be disturbed with the appearance of the external magnetic field, resulting in a redistribution of the these ferromagnetic nanoparticles in the suspension. Finally, they form linear chains or columns. Due to the contactless control of magnetic fields and fast response, magnetic field controllable assembly has been regarded as a convenient and efficient method to create ordered colloidal arrays and modulate their photonic properties. Much work has been carried out to study the magnetically controllable PCs through the self-assembly of colloidal spheres [19], where the charged polystyrene particles containing nanoscale iron oxide nanoparticles or the spinel ferrites material were synthesized through emulsion polymerization. And the lattice spacing can be altered by magnetic fields [22]. Due to the unique properties of SPCs, their wide applications include the magneto-optical devices [28, 29, 31–33], biomedical treatment [34, 35], cancer diagnosis [36] and hypothermal treatment [37].

In this review, we theoretically investigate the optical properties in 1D SPCs [38–42]. The proposed SPCs is composed of alternating ferrofluid layers and dielectric layers. Due to the magnetic field induced anisotropic property of ferrofluids, the photonic band gap can effectively be tuned with the initiation of an external magnetic field and the volume fraction of the nanoparticles. The absorption effect in the ferrofluids layer is considered with ferromagnetic nanoparticles coated with metallic layer. The complex wave vector results in the appearance of an additional band gap in the lower frequency region. Moreover, these band gaps blueshift when the external magnetic field is enhanced, and redshift when the thickness of metallic layer is increased. Graded ferrofluids layer in the SPCs is investigated through a varying number of deposited ferrofluids layers. Regarding each layer in the multilayer structure as a series of capacitance, the effective dielectric constant is derived. Numerical results have shown that the position and width of the photonic band gap can be effectively modulated by varying the number of graded composite layer, the volume fraction of nanoparticles and the external stimuli. Finally, the nonlinear optical response in the ferrofluids is studied, where ferromagnetic nanoparticles are coated by a nonmagnetic nanoshell with an intrinsic second-harmonic generation (SHG) susceptibility in a nonmagnetic host fluid. The SHG of such materials possess magnetic-field controllabilities, redshift, and enhancement.

This review is organized as follows. In Section 2, we introduce the transfer matrix method and the magnetic filed induced structure anisotropic factor α, which are frequently employed in our theoretical study. In Section 3, we study the magnetic field controllable photonic band gap in the SPCs with ferrofluids, see the original research work in Ref. [38]. In Section 4, the complex wave vector in the ferrofluids layer is investigated, where the ferromagnetic nanoparticle is coated with metallic layer, see the original research work in Ref. [39]. In Section 5, the graded multilayer structure of the ferrofluids is studied, see the original research work in Ref. [40]. In Section 6, the nonlinear optical materials with an enhanced SHG susceptibility is presented, see the original research work in Ref. [41]. This review ends with a summary in Section 7.

2 Fundamentals

2.1 Transfer matrix method

Under normal incidence, the schematic light pathway between two surfaces (surface I and surface II) with different refraction index is illustrated in Fig. 1, where n_i is the refraction index of the incident space, n_1 is the refraction index of material 1, n_o is the refraction index of the outgoing space. The incident beam undergoes an external reflection at the first interface I, and the transmitted beam undergoes an internal reflection and transmission at the second interface II. Dynamic properties of the

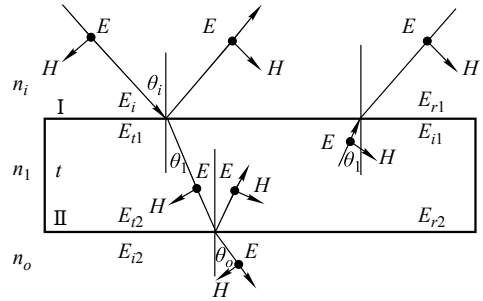

Fig. 1 Schematic view of the light pathway between two surfaces (surface I and surface II) with different refraction index is shown. n_i is the refraction index of the incident space, n_1 is the refraction index of material 1, n_o is the refraction index of the outgoing space. Under normal incidence, the incident beam undergoes an external reflection at the first interface I and the transmitted beam undergoes an internal reflection and transmission at the second interface II. The components of the E and H field are also illustrated.

electric field and magnetic field are contained with boundary conditions. Namely, normal components of $D(B)$ and tangential components of $E(H)$ are continuous, which can be explicitly expressed as [43, 44]

$$E_{\rm I} = E_i + E_{r1} = E_{t1} + E_{i1}$$
$$E_{\rm II} = E_{i2} + E_{r2} = E_{t2} \quad (1)$$
$$H_{\rm I} = H_i\cos\theta_i - H_{r1}\cos\theta_i = H_{t1}\cos\theta_1 - H_{i1}\cos\theta_1$$
$$H_{\rm II} = H_{i2}\cos\theta_1 - H_{r2}\cos\theta_1 = H_{t2}\cos\theta_o \quad (2)$$

where E_i is the incident electric field, $E_{r1}(E_{t1})$ is the reflected (transmitted) electric filed at interface I, $E_{r2}(E_{t2})$ is the reflected (transmitted) electric filed at interface II. The definition of the H filed is the same as that of the E field. Using the relation $H = nE\sqrt{\epsilon_0/\mu_0}$ and the boundary conditions Eq. (2), the magnetic field can be written as a function of the electric field:

$$H_{\rm I} = \sqrt{\epsilon_0/\mu_0}n_i\cos\theta_i(E_i - E_{r1})$$
$$= \sqrt{\epsilon_0/\mu_0}n_1\cos\theta_1(E_{t1} - E_{i1}) \quad (3)$$
$$H_{\rm II} = \sqrt{\epsilon_0/\mu_0}n_1\cos\theta_1(E_{i2} - E_{r2})$$
$$= \sqrt{\epsilon_0/\mu_0}n_o\cos\theta_o E_{t2} \quad (4)$$

Assuming $\eta = n\sqrt{\epsilon_0/\mu_0}$, thus $\eta_i \equiv n_i\cos\theta_i\sqrt{\epsilon_0/\mu_0}$, $\eta_1 \equiv n_1\cos\theta_1\sqrt{\epsilon_0/\mu_0}$ and $\eta_o \equiv n_o\cos\theta_o\sqrt{\epsilon_0/\mu_0}$. Eq. (3) and Eq. (4) can be simplified as

$$H_{\rm I} = \eta_i(E_i - E_{r1}) = \eta_1(E_{t1} - E_{i1})$$
$$H_{\rm II} = \eta_1(E_{i2} - E_{r2}) = \eta_o E_{t2} \quad (5)$$

Additionally, there is a phase difference δ between E_{i2} and E_{t1}, where $\delta = k_i\Delta = (2\pi/\lambda)n_i t\cos\theta_{t1}$. Thus, $E_{i2} = E_{t1}\mathrm{e}^{-\mathrm{i}\delta}$ and $E_{i1} = E_{r2}\mathrm{e}^{-\mathrm{i}\delta}$. Substitute E_{i2} and E_{i1} into Eq. (1) and Eq. (5), we can get the following relations,

$$E_{\rm I} = E_{\rm II}\cos\delta + H_{\rm II}\mathrm{i}\sin\delta/\eta_1$$
$$H_{\rm I} = E_{\rm II}\mathrm{i}\eta_1\sin\delta + H_{\rm II}\cos\delta \quad (6)$$

Rewritten them in matrix form,

$$\begin{pmatrix} E_{\rm I} \\ H_{\rm I} \end{pmatrix} = \begin{pmatrix} \cos\delta & \mathrm{i}\sin\delta/\eta_1 \\ \mathrm{i}\eta_1\sin\delta & \cos\delta \end{pmatrix}\begin{pmatrix} E_{\rm II} \\ H_{\rm II} \end{pmatrix}$$
$$= M\begin{pmatrix} E_{\rm II} \\ H_{\rm II} \end{pmatrix} \quad (7)$$

where

$$M = \begin{pmatrix} \cos\delta & \mathrm{i}\sin\delta/\eta_1 \\ \mathrm{i}\eta_1\sin\delta & \cos\delta \end{pmatrix} \quad (8)$$

Now the characteristic equation between two layers is obtained [Eq. (7)]. Each layer of the multilayers has its own transfer matrix and the overall transfer matrix of the N periods PCs is the product of individual transfer matrices. For N unit layer, it leads to the matrix equation,

$$M = \prod_i^N M_i \quad (9)$$

Using the boundary conditions, the transfer matrix could be rewritten in the form:

$$M = \begin{pmatrix} m_{11} & m_{12} \\ m_{21} & m_{22} \end{pmatrix} \quad (10)$$

The coefficients of reflection and transmission are defined as

$$t = \frac{2\eta_i}{\eta_i m_{11} + \eta_i\eta_o m_{12} + m_{21} + \eta_o m_{22}} \quad (11)$$
$$r = \frac{\eta_i m_{11} + \eta_i\eta_o m_{12} - m_{21} - \eta_o m_{22}}{\eta_i m_{11} + \eta_i\eta_o m_{12} + m_{21} + \eta_o m_{22}} \quad (12)$$

These expressions can be used for any number of layers in PCs to determine the coefficients of transmission ($T = |t|^2$) and reflection ($R = |r|^2$) [2, 45].

For the 1D PCs with double layers, the dispersion relation admits the following form

$$\cos(kd) = \cos(k_1 d_1)\cos(k_2 d_2)$$
$$-\frac{1}{2}\left(\frac{k_1}{k_2} + \frac{k_2}{k_1}\right)\sin(k_1 d_1)\sin(k_2 d_2) \quad (13)$$

which is got by solving the non-zero solution of $\det\,(M - \mathrm{e}^{-\mathrm{i}kd}) = 0$ [46]. where $d_1(d_2)$ is the thickness of corresponding layers. d is the lattice constant and $d = d_1 + d_2$. k represents the wave vector in the PCs, $k_1 = \omega\sqrt{\epsilon_1}/c$ denotes the local wave vector of layer 1, and $k_2 = \omega\sqrt{\epsilon_2}/c$ is the local wave vector of layer 2. ω is the frequency of light or electromagnetic waves, and c is the speed of light in vacuum.

2.2 Magnetic structure anisotropic factor

For the ferrofluids, ferromagnetic nanoparticles around 10 nm in diameter randomly distributed in the suspension. When the external magnetic field (H) was applied, ferromagnetic nanoaprticles will align along the field direction, thus changing the microstructure of the system correspondingly [47–53]. The schematic structure of the ferromagnetic nanoparticle under the influence of the magnetic field is shown in Fig. 2.

Let α represent the field induced structure anisotropic factor. In detail, α denotes the local field factors $\alpha_\parallel$ and $\alpha_\perp$ for longitudinal and transverse field cases, respectively [54]. Here the longitudinal (or transverse) field case corresponds to the fact that the E-field of the light is parallel (or perpendicular) to the particle chain. There is a

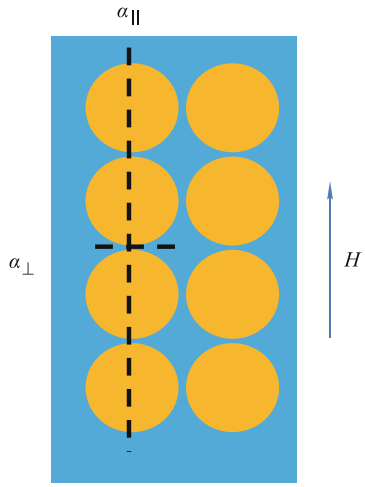

Fig. 2 Ferromagnetic nanoparticles under the influence of the external magnetic field H is illustrated. And these ferromagnetic nanoparticle form chains along the H direction. α is the magnetic field induced structure anisotropic factor. It has the longitudinal $\alpha_{\parallel}$ and $\alpha_{\perp}$ perpendicular components respectively.

sum rule for $\alpha_{\parallel}$ and $\alpha_{\perp}$, $\alpha_{\parallel} + 2\alpha_{\perp} = 3$. The parameter α measures the degree of anisotropy induced by the applied magnetic field H [55]. More precisely, the degree of the field-induced anisotropy is measured by how much α deviates from unity, $0 < \alpha_{\parallel} < 1$ for transverse field cases and $1 < \alpha_{\perp} < 1.5$ for longitudinal field cases. As H increases $\alpha_{\parallel}$ and $\alpha_{\perp}$ should tend to 0 and 1.5, respectively, which is indicative of the formation of more and more particle chains as evident in experiments.

A crude estimate of α can be obtained from the contribution of chains, namely,

$$\alpha = \frac{1}{\phi}\sum_{k=1}^{n} kV_0V_k(H)N_k \tag{14}$$

where ϕ denotes the volume fraction of the structured particles in the suspension, N_k the depolarization factor for a chain with k structured particles, V_0 the volume of one particle in suspension (considered to be spherical and all identical), and $V_k(H)$ the density of the chain which is a function of H [56, 57]. It is noteworthy that for given ϕ, $V_k(H)$ also depends on the dipolar coupling constant which relates the dipole–dipole interaction energy of two contacting particles to the thermal energy. Specifically, if there is no external magnetic field $H = 0$, the magnetic moments within the ferrofluids particles are randomly distributed, which indicates that no net measurable magnetization can be obtained. It leads to $\alpha_{\parallel} = \alpha_{\perp} = 1$. But when an external magnetic field is applied, the magnetic moments of the particles orient along the field direction of the externally applied field. It means that the alignment of magnetic moments is very sensitive to the external magnetic field [58]. Therefore, α should be a function of external magnetic fields H.

3 Magneto-controllable SPCs based on ferrofluids

Here we present a class of magneto-controllable SPCs based on ferrofluids [38]. The proposed structure is composed of alternating ferrofluid layers and dielectric layers. Periodic array of dielectric scatters and the observation of the strong localization of photons are the essential properties of PCs in analogy to the allowed (forbidden) energy bands (gaps) of semiconductors [59]. This funny field has inspired great interest in recent years because of their potential ability to control the propagation of electromagnetic waves or modify the density of electromagnetic states inside the crystal [14, 60, 61]. PCs with complete band gaps have many applications [62], including the fabrication of lossless dielectric mirrors and resonant cavities for light [63]. In addition, the visibility of graphene layers was found to be enhanced greatly when one-dimensional (1D) PCs were added [64], and the linear and nonlinear optical properties of 1D PCs containing ZnO defects were also studied [65]. Recently the electric tunability of PCs with nonlinear composites was theoretically explored [66]. Experimentally, magnetic-field tunable photonic stop bands in a stack of containers with magnetizable ferromagnetic spheres were studied [67]. Colloidal photonic crystals, which were magnetically fabricated by using superparamagnetic magnetite-nanocrystal clusters, can also realize stop bands covering the entire visible spectrum [68]. Usually a tunable band gap in PCs is achieved by varying the lattice constant or symmetry of the perfectly ordered crystal by using different methods such as elastic stress (structure transformation) [69], temperature tuning [70], femtosecond direct writing technique [71] or magnetic (electric) fields [67, 72]. Meanwhile, the following developments in PCs are also very fascinating, such as tunable photonic band in two-dimensional photonic crystal slab waveguides by atomic layer deposition [73], tunability of PCs due to the electrically induced birefringence of the twisted dielectric grains [74] and electrical tuning of three-dimensional photonic crystals using polymer-dispersed liquid crystals [75]. In this section we exploit a class of magneto-controllable 1D SPCs, which are made of colloidal ferrofluids.

3.1 Formulism

For 1D SPCs with double layers (see Fig. 3), the local field factor induced by the external magnetic field in the suspension can be obtained by the Ewald Kornfeld formula [54]. If there is no special instructions, we shall use α to denote both $\alpha_{\perp}$ and $\alpha_{\parallel}$ in the following. Here we

consider the cobalt nanoparticles suspended in the water.

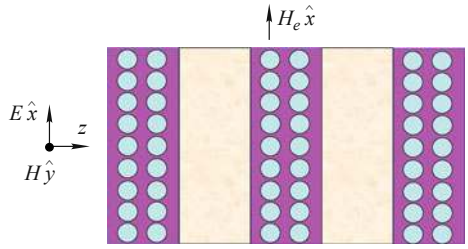

Fig. 3 Schematic graph showing one-dimensional soft photonic crystals (1D SPCs) containing periodic double layers, one of which is a ferrofluid layer (layer 1) and the other of which is a dielectric layer (layer 2). In the ferrofluid layer, ferromagnetic spherical nanoparticles (in circle) are embedded in a carrier fluid in the presence of x-directed external magnetic field H_e. An electromagnetic wave is incident on the 1D SPCs along the z axis, whose electric-field (E) and magnetic-field (H) components are directed along the x and y axes, respectively. For model calculations, we take layer 2 to be air, the carrier fluid to be water, and the suspended nanoparticles to be cobalt. Reproduced from Ref. [38].

Due to the different polarization of the incident light, the effective dielectric constant of the composite ϵ_e will be $\epsilon_\perp$ or $\epsilon_\parallel$. Here we use ϵ to represent $\epsilon_\perp$ and $\epsilon_\parallel$, which can be given through the wellknown Maxwell–Garnett theory [55, 76–78]:

$$\frac{\epsilon_e-\epsilon_2}{\alpha\epsilon_e+(3-\alpha)\epsilon_2}=p\frac{\epsilon_1-\epsilon_2}{\epsilon_1+2\epsilon_2} \tag{15}$$

where p is the volume fraction of the nanoparticles in the composite suspension. ϵ_1 is the dielectric constant of the nanoparticles. ϵ_2 is the dielectric constant of host fluid (water). Here we take ϵ_1 of the cobalt nanoparticles as $-13.1704\epsilon_0$, which is characterized by using the incident wavelength $\lambda=661$ nm [79], and the dielectric constant of water is $1.77\epsilon_0$. From Eq. (15) we know the anisotropy factor α induced in this composite has a direct effect on the effective dielectric constant of the composite. Thus, the refractive index of this layer is tuned correspondingly.

Then we use the transfer matrix method [80] to study the band structures of 1D periodic photonic structures. For 1D SPCs with double layers, the dispersion relation is in the form as

$$\cos(kd)=\cos(k_1d_1)\cos(k_2d_2)-\frac{1}{2}\left(\frac{k_1}{k_2}+\frac{k_2}{k_1}\right)\sin(k_1d_1)\sin(k_2d_2) \tag{16}$$

where $d_1(d_2)$ is the thickness of corresponding layers. Here we take layer 1 as the ferrofluid composites and layer 2 as the air. d is the lattice constant and $d=d_1+d_2$. k represents the wave vector in the PCs, $k_1=\omega\sqrt{\epsilon_1}/c$ denotes the local wave vector of layer 1, and $k_2=\omega\sqrt{\epsilon_2}/c$ is the local wave vector of layer 2. ω is the frequency of light or electromagnetic waves, and c is the speed of light in vacuum. The dielectric constant of air is taken as $\epsilon_2=\epsilon_0$.

3.2 Numerical results and discussions

Now we are in a position to do numerical calculations in our proposed 1D SPCs. Figure 4 shows the calculated band structure of the model system. When the magnitude of the applied magnetic field H_e increases from zero to a large value (namely, the longitudinal local H_e factor $\alpha_\parallel$ changes from 1.0 to 0.2), we find that H_e has a significant effect on the band gaps and causes them to move towards a higher frequency region (blue shift). Next, we display the first band gap width Δ in Fig. 5. The Δ is shown to get larger when $\alpha_\parallel$ approaches zero step by step. Alternatively, the band gap width is caused to increase when the magnitude of the external magnetic field H_e increases.

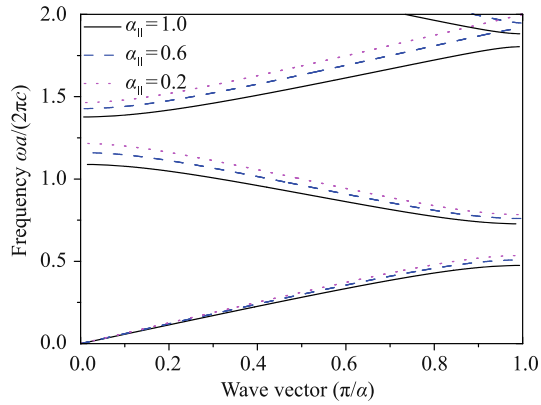

Fig. 4 Band structure of the model 1D SPCs (Fig. 3) for different $\alpha_\parallel$. Parameters: $p=0.25$ and $d_1=d_2=0.5a$. Reproduced from Ref. [38].

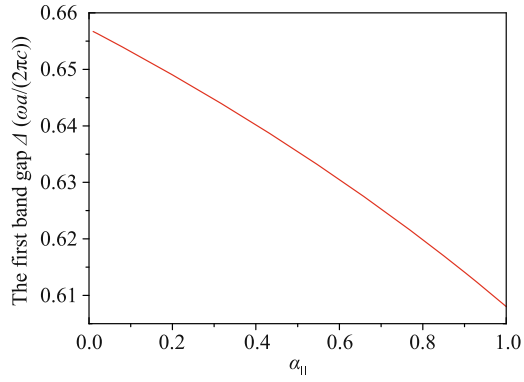

Fig. 5 The first band gap width of the model 1D SPCs (Fig. 3) vs. $\alpha_\parallel$. Parameters: $p=0.25$ and $d_1=d_2=0.5a$. Reproduced from Ref. [38].

Figure 6 shows the cobalt concentration effect on the band structure of the model 1D SPCs. In this case, we set $H_e=0$. When p gets larger (i.e., the ferrofluid becomes denser), the first and second band gaps get wider and move towards the lower frequency region (red shift).

Here, $p = 0$ represents the case that there are no cobalt nanoparticles. In this case, the band gaps are caused to appear by the combination of pure-water layers and air layers. Our results show that the composite effect in ferrofluid layers plays an important role as p is non-zero. In such cases, if an external magnetic field H_e is applied, it can lead to a tunable effective dielectric constant (or refractive index) of the ferrofluid layer, thus yielding magneto-controllable band gaps.

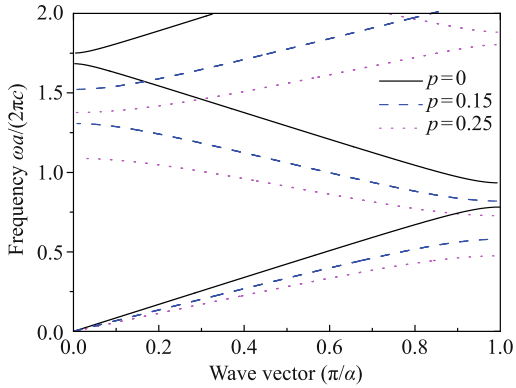

Fig. 6 Band structure of the model 1D SPCs for various volume fraction p. Parameters: $\alpha_{\parallel} = 1$ and $d_1 = d_2 = 0.5a$. Here, $\alpha_{\parallel} = 1$ represents that there is no external magnetic field H_e. Reproduced from Ref. [38].

In this section, we have only calculated the case of the E component being parallel with the nanoparticle chain, i.e., longitudinal E case. For the transverse E case, the corresponding band gaps can also be tuned. However, for the same H_e, the tunability for the transverse E case is less and opposite, due to the existence of the sum rule $\alpha_{\parallel} + 2\alpha_{\perp} = 3$. In addition, the formation of nanoparticle chains can be weakly affected by the application of incident electromagnetic waves (e.g., of light [81].) Apparently, this does not affect the present results at all.

4 Magneto-controllable SPCs with the incorporation of the absorption effect

Until now one-dimensional, two-dimensional, and three-dimensional PCs have been widely studied [82–84]. Theoretically, the plane wave expansion [85], the transfer matrix [86], and the finite difference time methods [87] have been well developed to study the propagational properties of photons. Experimentally, the lithography [88, 89], the self-assembly [11], and the colloidal crystal template methods are developed for fabrication of PCs with well controlled structure [90]. Among them, the ability to get tunable band gap is a topic of much interest, which is originated from the variation of refractive index or the symmetry of materials. With the utilization of composite microstructures [91] tunable photonic band gaps can be realized by different external factors such as an electric [92], magnetic field [38], temperature [93] or mechanical force [94]. Mostly, each component of PCs is a nonabsorbent material, so the wave vector in the system is frequency independent. If the metallic part is inserted in the periodic structure, the pathway of the electromagnetic field will be different [95–97]. Here we investigate the 1D SPCs based on ferrofluids with consideration of the absorption effect, where the ferromagnetic nanoparticles coated by the metallic layer (see Fig. 7). It is composed of a ferrofluids layer and an air layer. a is the thickness of the ferrofluids layer, and b is the thickness of the air. The filling factor representing the ratio of the ferrofluids in the lattice is defined as $\nu = a/d$. For the air layer, the refraction index is taken as 1.0.

In our model system, ferromagnetic linear nanoparticles of linear dielectric constant coated with a nonmagnetic metallic nonlinear shell are investigated in ferrofluids. New nanoparticles (magnetic-metallic composite) combining an optical signature with magnetic response are particularly useful [98–101]. For the magnetic-non metallic shell, they are coated by stabilizing surfactant layers to prevent the aggregation of the nanosized magnetic particle under van der Waals forces. To investigate the EM wave propagation in this magnetic field induced anisotropic structure, we choose the magnetic-metallic core-shell structure. Synthesis of the metallic (Au, Ag) coated cobalt nanoparticles can be realized by partial replacement reaction [35, 102, 103]. Through this homogeneous non-aqueous approach, magnetic core-metallic shell composite forms the stable ferrofluids.

4.1 Formulism

We theoretically investigate the properties of optical propagation in one-dimensional SPCs based on ferrofluids by using the transfer matrix method. Specifically, ferrofluids are composed of the suspended ferromagnetic nanoparticles coated with silver, which has a frequency dependent dielectric function. Incorporation of the absorption effect in the 1D SPCs, the complex wave vector can be expressed as [104]

$$\cos(Kd) = f_1(\omega) + \mathrm{i}f_2(\omega) \tag{17}$$

where K represents the complex wave vector. d is the lattice constant. $f_1(\omega)$ and $f_2(\omega)$ denote the real and imaginary part, respectively. To get the expression of $f_1(\omega)$ and $f_2(\omega)$, we transform Eq. (16) as the following:

$$\cos(Kd) = \cos\left(n_1\frac{\omega a}{c}\right)\cos\left(n_2\frac{\omega b}{c}\right) - \frac{1}{2}\left(\frac{n_1}{n_2} + \frac{n_2}{n_1}\right)\sin\left(n_1\frac{\omega a}{c}\right)$$

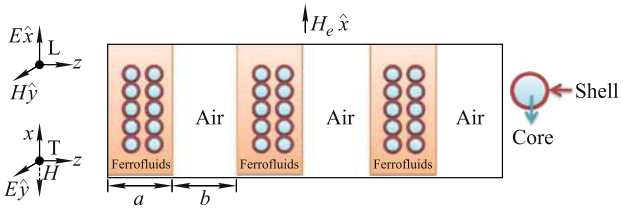

Fig. 7 Schematic view of 1D SPCs, composed of alternating ferrofluid layers and dielectric layers. For the ferrofluids, the ferromagnetic nanoparticles are suspending in the host liquid. Here we take it as the cobalt nanoparticles (core) coated by the silver (shell). When an external magnetic filed H_e is applied, the core-shell nanoparticles will align along the magnetic field direction and form chains. An electromagnetic wave is incident on the 1D SPCs along the z axis, whose electric-field E and magnetic-field H components are directed along the x and y axes for the longitudinal (L) field cases, and along the y and $-x$ direction for the transverse (T) field cases. The thickness of the ferrofluids layer is a. The thickness of the air layer is b. Hence, the lattice constant is $d = a + b$. Reproduced from Ref. [39].

$$\times \sin\left(n_2\frac{\omega b}{c}\right) \tag{18}$$

For simplicity, we take the dielectric layer 2 as air in our calculation; actually we can also take it as SiO_2, ZnSe, $GaAs$ and so on. Substitute $n_1 = n_r + \mathrm{i}n_i$, $n_2 = 1$, $\xi_r = \mathrm{Re}\left(n_1 + \frac{1}{n_1}\right)$ and $\xi_i = \mathrm{Im}\left(n_1 + \frac{1}{n_1}\right)$ into Eq. (18). It becomes

$$\begin{aligned}\cos(Kd) = {} & \cos\left((n_r + \mathrm{i}n_i)\frac{\omega a}{c}\right)\cos\left(\frac{\omega b}{c}\right) \\ & -\frac{1}{2}(\xi_r + \mathrm{i}\xi_i)\sin\left((n_r + \mathrm{i}n_i)\frac{\omega a}{c}\right) \\ & \times \sin\left(\frac{\omega b}{c}\right)\end{aligned} \tag{19}$$

Simplify Eq. (19), and we finally get

$$\begin{aligned}\cos(Kd) = {} & \left[\cos\left(n_r\frac{\omega a}{c}\right)\cosh\left(n_i\frac{\omega a}{c}\right)\right. \\ & \left.-\mathrm{i}\sin\left(n_r\frac{\omega a}{c}\right)\sinh\left(n_i\frac{\omega a}{c}\right)\right]\cos\left(\frac{\omega b}{c}\right) \\ & -\frac{1}{2}(\xi_r + \mathrm{i}\xi_i)\times\sin\left(\frac{\omega b}{c}\right) \\ & \times\left[\sin\left(n_r\frac{\omega a}{c}\right)\cosh\left(n_i\frac{\omega a}{c}\right)\right. \\ & \left.+\mathrm{i}\cos\left(n_r\frac{\omega a}{c}\right)\sinh\left(n_i\frac{\omega a}{c}\right)\right]\end{aligned} \tag{20}$$

Thus,

$$\begin{aligned}f_1(\omega) = {} & \cos\left(n_r\frac{\omega a}{c}\right)\cosh\left(n_i\frac{\omega a}{c}\right)\cos\left(\frac{\omega b}{c}\right) \\ & -\frac{1}{2}\xi_r\sin\left(\frac{\omega b}{c}\right)\sin\left(n_r\frac{\omega a}{c}\right)\cosh\left(n_i\frac{\omega a}{c}\right) \\ & +\frac{1}{2}\xi_i\sin\left(\frac{\omega b}{c}\right)\cos\left(n_r\frac{\omega a}{c}\right) \\ & \times\sinh\left(n_i\frac{\omega a}{c}\right)\end{aligned} \tag{21}$$

$$\begin{aligned}f_2(\omega) = {} & -\sin\left(n_r\frac{\omega a}{c}\right)\sinh\left(n_i\frac{\omega a}{c}\right)\cos\left(\frac{\omega b}{c}\right) \\ & -\frac{1}{2}\xi_r\sin\left(\frac{\omega b}{c}\right)\cos\left(n_r\frac{\omega a}{c}\right)\sinh\left(n_i\frac{\omega a}{c}\right) \\ & -\frac{1}{2}\xi_i\sin\left(\frac{\omega b}{c}\right)\sin\left(n_r\frac{\omega a}{c}\right) \\ & \times\cosh\left(n_i\frac{\omega a}{c}\right)\end{aligned} \tag{22}$$

As we know, the real part of the complex wave vector K, namely k_r, corresponds to the wave number in the 1D SPCs, while the imaginary part k_i determines the absorption coefficient β. It can be expressed as

$$\beta = 2k_i \tag{23}$$

Simplify $\cos K$ by using $K = k_r + ik_i$ and we obtain

$$\begin{aligned}\cos K &= \cos(k_r + \mathrm{i}k_i) \\ &= \cos k_r \cosh k_i - \mathrm{i}\sin k_r \sinh k_i\end{aligned} \tag{24}$$

The real part of the photonic band structure for given wave number k_r can be found based on Eqs. (17) and (24) by seeking the frequencies ω which follow the equation:

$$\cos(k_r d) = f_1(\omega)\left[\frac{f_2^2(\omega)}{\sin^2(k_r d)} + 1\right]^{-1/2} \tag{25}$$

In our numerical calculations, the dielectric constant of the silver $\epsilon_1'(\omega)$ is a function of ω. It follows a Drude dielectric function, which is valid for noble metals within the frequency range of interest. $\epsilon_1'(\omega)$ can be expressed as [41]

$$\epsilon_1'(\omega) = \epsilon(\infty) - [\epsilon(0) - \epsilon(\infty)]\frac{\omega_p^2}{\omega(\omega + i\gamma)} \tag{26}$$

where ω_p is the bulk plasmon frequency, $\epsilon(\infty)$ is the high-frequency limit dielectric constant, $\epsilon(0)$ is the static dielectric constant, and γ is the collision frequency. Specifically, for silver, $\epsilon(\infty) = 5.45$, $\epsilon(0) = 6.18$, and $\omega_p = 1.72 \times 10^{16}\,\mathrm{rad/s}$ [105]. In addition, we take $\gamma = 0.01\omega_p$ (a typical value for metals). For the cobalt nanoparticle, we take $\epsilon_1'' = -25 + 4\mathrm{i}$. It should be reasonable to see the ϵ_1'' as frequency-independent, since it only varies very slightly with the frequency of external fields.

Thus, the equivalent linear dielectric constant $\epsilon_1(\omega)$ for the core-shell composite nanoparticle can be obtained through the Maxwell-Garnett formula [55, 106], which describes a two-component composite where many particles of the dielectric constant ϵ_p and the volume fraction v_p are randomly embedded in a host medium. Thus,

$$\frac{\epsilon_1(\omega) - \epsilon_1'(\omega)}{\epsilon_1(\omega) + 2\epsilon_1'(\omega)} = (1 - f)\frac{\epsilon_1'' - \epsilon_1'(\omega)}{\epsilon_1'' + 2\epsilon_1'(\omega)} \tag{27}$$

where f is the volume ratio of the nanoshell to the whole coated nanoparticle. It equals to $f = 1 - r^3/R^3 = 1 - t^3$. Shell thickness parameter $t = r/R$, where r relates to the radius of the magnetic core. R is the radius of the core-shell composites. The thinner the shell layer, the larger t is. The Maxwell-Garnett formula follows a well-known asymmetrical effective medium theory, and may thus be valid for a low concentration of nanoparticles in the composites [107].

The effective linear dielectric constant of the whole suspension under the present consideration $\epsilon_e(\omega)$ can be given by the developed Maxwell-Garnett approximation which works for suspensions with field-induced anisotropic structures [106]:

$$\frac{\epsilon_e(\omega) - \epsilon_2}{\alpha\epsilon_e(\omega) + (3-\alpha)\epsilon_2} = p\frac{\epsilon_1(\omega) - \epsilon_2}{\epsilon_1(\omega) + 2\epsilon_2} \tag{28}$$

ϵ_2 is a frequency-independent dielectric constant of the host liquid, and $\epsilon_2 = 1.77$ for water. The volume fraction of the nanoparticles in the suspension is p, and here we take $p = 0.18$. The parameter α measures the degree of structural anisotropy due to the formation of nanoparticle chains, which are induced by the external magnetic field H_e. The aim of the intended introduction of α into Eq. (28) is to include the field-induced anisotropy in the system, at least qualitatively. In detail, α denotes the local field factors, $\alpha_\parallel$ and $\alpha_\perp$ for longitudinal and transverse field cases, respectively. Schematic structure of the local magnetic field anisotropy factor $\alpha_\parallel$ and $\alpha_\perp$ is shown in Fig. 8. As for the refracitve index n_1 of the ferrofluids layer, it can be easily obtained from expression $n_1 = \sqrt{\epsilon_e}$, where ϵ_e is the effective dielectric constant of the ferrofluids layer. Thus, $n_r = \mathrm{Re}(\sqrt{\epsilon_e})$ and $n_i = \mathrm{Im}(\sqrt{\epsilon_e})$.

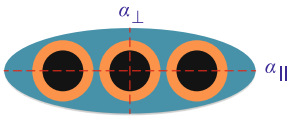

Fig. 8 Schematic graph shows the local magnetic factor along the major ($\alpha_\parallel$) or minor axis ($\alpha_\perp$) respectively. The whole nanoparticles chain can be treated as an equivalent spheroid. Reproduced from Ref. [39].

4.2 Numerical results and discussions

Figure 9 shows the absorption coefficient $\log_{10}(10^6\beta)$ of 1D SPCs as a function of the frequency $\omega d/(2\pi c)$. When the external magnetic field H_e is applied, the coated nanoparticles will form chains along the magnetic field direction changing the microstructure of the system accordingly. For the sake of numerical calculations, we take $t = 0.5$ and $\nu = 0.5$. First, we consider the longitudinal (L) field cases as shown in Fig. 9. When the local magnetic factor $\alpha_\parallel$ gradually decreases from 1.0 to 0.02, the structure anisotropy induced by the external magnetic field makes the dispersion curve blueshift (moving to the high frequency region). Meanwhile the absorption coefficient decreases and the absorption curves are not continuous. To fully understand the origin of such phenomena we can take a look at the inset Figs. 9 (a) and (b). Inset (a) shows the real part of the complex wavevector $k_r d/\pi$ as a function of the frequency. An additional band gap appears due to the dissipation coefficient γ in Eq. (26) in the low frequency region. Now let us take a look at the distribution of $f_1(\omega)$ as a function of frequency, which is shown as inset (b). It represents the real part of the complex wave vector $\cos(Kd)$, and its oscillation defines the frequency regions in which the argument Kd takes real values (the regions where $|f_1(\omega)| \leqslant 1$). In other words, the band gaps happen in the frequency region where $|f_1(\omega)| > 1$. When $\alpha_\parallel$ gradually decreases, the distribution of $f_1(\omega)$ blueshift (moving to the higher frequency region). For the transverse (T) field cases the behaviors of the dispersion curve is similar to those for L field cases (not shown here). Thus, the enhanced magnitude of the external magnetic filed ($\alpha_\parallel$ decreases or $\alpha_\perp$ increases) causes the band gaps of 1D SPCs blueshift.

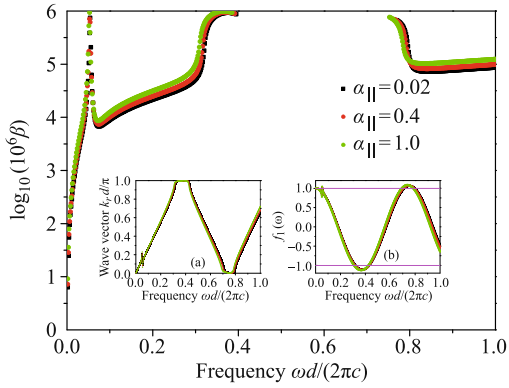

Fig. 9 For the L field cases, the absorption coefficient $\log_{10}(10^6\beta)$ as a function of the frequency $\omega d/(2\pi c)$ for various $\alpha_\parallel$. Inset **(a)** the dispersion relation of the wave vector $k_r d/\pi$, inset **(b)** real part of $\cos(Kd)$, namely, $f_1(\omega)$. The square, circle and triangular dots are corresponding to $\alpha_\parallel = 0.02, 0.4, 1.0$ respectively. Parameters: $t = 0.5$ and $\nu = 0.5$. Reproduced from Ref. [39].

Figure 10 demonstrates the absorption coefficient $\log_{10}(10^6\beta)$ of 1D SPCs as a function of the frequency $\omega d/(2\pi c)$ depending on the thickness parameter t. For the L field cases, $\alpha_\parallel = 0.4$ and $\nu = 0.5$. When the thickness of the shell increases, t will decrease. From Fig. 10, one can clearly see that band gaps shift to the low frequency region when t increases from 0.1, 0.3, to 0.8. That means, the thinner shell layer of silver gives rise to the redshift of band gaps. Also the larger t leads to higher absorption coefficient $\log_{10}(10^6\beta)$. Inset (a) illustrates the distribution of $k_r d/\pi$ as a function of frequency. These band gaps in Fig. 10 are caused by the frequency range

where $|f_1(\omega)| > 1$ as shown in inset (b).

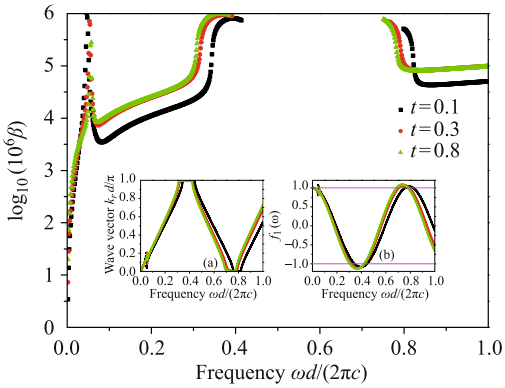

Fig. 10 For the L field cases, the absorption coefficient $\log_{10}(10^6\beta)$ as a function of the frequency $\omega d/(2\pi c)$ for various t. Inset **(a)** the dispersion relation of the wave vector $k_r d/\pi$, inset **(b)** real part of $\cos(Kd)$, namely, $f_1(\omega)$. The square, circle and triangular dots are corresponding to $t = 0.1, 0.3, 0.8$ respectively. Parameters: $\alpha_\parallel = 0.4$ and $\nu = 0.5$. Reproduced from Ref. [39].

The influence of filling factor ν on the dispersion curve is illustrated in Fig. 11. Here we keep the parameters $\alpha_\parallel = 0.4$ and $t = 0.5$. By tuning the filling factor ν from 0.1, 0.3 to 0.5, we can find a redshift (moving to the low frequency region) of the band gap of the 1D SPCs as shown in Fig. 11. It is evident that the absorption coefficient becomes larger when ν increases (Fig. 11). The distribution of $k_r d/\pi$ and $f_1(\omega)$ are shown as inset (a) and (b) respectively.

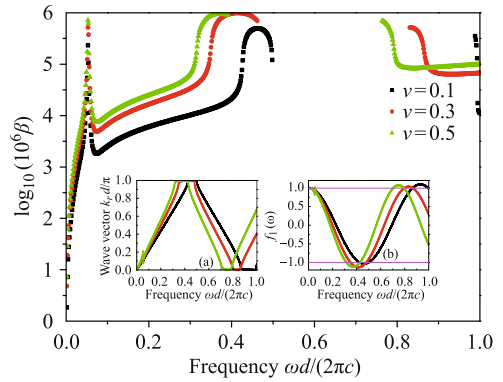

Fig. 11 For the L field cases, the absorption coefficient $\log_{10}(10^6\beta)$ as a function of the frequency $\omega d/(2\pi c)$ for various ν. Inset **(a)** the dispersion relation of the wave vector $k_r d/\pi$, inset **(b)** real part of $\cos(Kd)$, namely, $f_1(\omega)$. The square, circle and triangular dots are corresponding to $\nu = 0.1, 0.3, 0.5$ respectively. Parameters: $\alpha_\parallel = 0.4$ and $t = 0.5$. Reproduced from Ref. [39].

We have also determined the variation of the band gap width as a function of the local magnetic factor α, the thickness ratio t and the filling factor ν of the ferrofluids layer. The band gap width tends to increase when the magnitude of the local magnetic factor $\alpha_\parallel$ decreases or t increases (not shown here). Specifically, the band gap width variation as a function of filling factor ν are shown in Fig. 12(a) for the L field case where $\alpha_\parallel = 0.4$, $t = 0.5$. ν is taken from 0.0 to 1.0. It can be observed that the variation of the second band gap width is closely related to ν. It got increased when ν is smaller than 0.35, but when ν is larger than 0.35 the width is reduced. The situation is the same for the T field case as shown in Fig. 12(b).

Based on the transfer matrix method, we theoretically studied the complex wave vector in 1D SPCs, which are composed of the periodic ferrofluids layer and air layer. The behavior in the 1D SPCs is quite different from the real wave vector in the PCs. Numerical results show that structure anisotropy induced by the external magnetic field causes the dispersion curve to blueshift when $\alpha_\parallel$ approaches 0.0, or $\alpha_\perp$ is close to 1.5. Also by increasing the thickness parameter t and the filling factor ν the band gaps will redshift. These band gaps in this proposed 1D SPCs structure are caused by the oscillating $f_1(\omega)$ within the frequency region where $|f_1(\omega)| > 1$. An additional band gap occurs in the low frequency region due to the dissipation factor γ in the dielectric function of silver. Also the band width variations are calculated. Our results presented in this section provide a guideline for designing the potential photonic devices based on the ferrofluids and it is helpful for improving the quality of these devices.

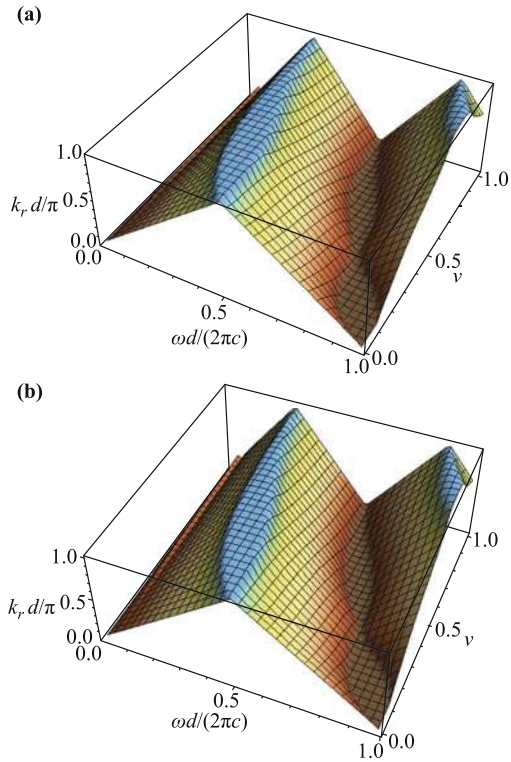

Fig. 12 3D illustration of the dispersion relation $k_r d/\pi$ as a function of the ferrofluids filling fraction ν and frequency $\omega d/(2\pi c)$. For the filling factor, ν is taken from 0.01 to 1.0. **(a)** for the L field cases, $\alpha_\parallel = 0.4$. **(b)** for the T field cases, $\alpha_\perp = 1.2$. Parameter: $t = 0.5$. Reproduced from Ref. [39].

5 1D graded SPCs with multilayer structure

PCs have attracted wide research attention owing to their unique light manipulation abilities, demonstrating wide applications in optical sensor, optical filter and various optical integrated circuit devices [5]. To fabricate them, both top down (lithographic technique) and bottom up method (nanoscale self-assembled method) [108] have been put forward to realize different structures like the slab [109], multilayer [110], cylinders array [111], or even the fractal structures [112]. Among them, one most studied structure is in the form of planar films [113], where the periodic alternating layers is obtained by bottom-up assembly. This procedure is based on sequential spin-coating suspensions of nanoparticles on the substrates. With such a method, simple, stable, inexpensive PCs are obtained. Meanwhile, modulation of the refractive index is achieved by alternating the size, type, concentrations of nanoparticles in composite layer or by controlling the number of the deposited layers [114, 115]. Moreover, PCs are able to be realized through a combination with channels, walls, or microfluidic chips [116], where colloids are forced through the area with pressure. In most cases, the composite layer is a suspension of monodispersed colloid, constituted by dielectric SiO_2 or TiO_2 particles [114, 117]. If small metallic nanoparticles are introduced into a suspension, the third order Kerr-type nonlinearity of composites have to be included, resulting in an enhancement in the local electric field [55, 92]. Simulation results have shown that tunable plasmon resonant effects arise with gold nanoparticles inserted into a periodic PCs [118].

Here we study the optical properties in 1D SPCs with graded multilayer. Graded materials are the ones whose material properties are spatial dependent. It has long been recognized that gradients in layer composition can improve the performance of a material [119–121], and open up the additional possibility of shaping the refractive contrast [122–124]. Let us consider a graded multilayer structure with N layers, the dielectric constant vary continuously along the z direction and in the ith layer the dielectric constant is expressed as $\epsilon_{(i,z)}$. The schematic structure of our proposed 1D GSPCs is illustrated in Fig. 13. It is composed of one composite layer and one air layer. Three layers with different nanoparticle volume fraction to represent the graded composite layer in Fig. 13. Specificly, Ag nanoparticle embedded in the TiO_2 is studied in the composite layer.

5.1 Formulism

For 1D PCs with an infinite period, the whole structure can be regarded as an series of multilayer structure, acting as a LC circuit. The reciprocal of the equivalent capacitance (C_{eqv}) of multiple capacitors connected in series is the sum of the reciprocals of the individual capacitances (C_n). It can be expressed as $1/C_{eqv} = 1/C_1 + 1/C_2 + \cdots + 1/C_n = \sum_{i=1}^{n}(1/C_n)$, where $C = \epsilon s/(4\pi k_c d_s)$. ϵ is the dielectric constant, s is the capacitor plates of area, d_s is the distance between capacitor plates, k_c is the electrostatic constant. Thus, by using the equivalent capacitance of series combination, the optical response of the graded composite layer ϵ_1 can be expressed as

$$\frac{1}{\epsilon_1} = \frac{1}{L}\int_0^L \frac{\mathrm{d}z}{\epsilon_i(i,z)} \tag{29}$$

where L is the thickness of the graded film, and it is divided into N layers. Due to the periodicity of the two refractive index materials, the multilayer structure creates a periodic potential for photons in one dimension. Electromagnetic waves of a given frequency propagating through a stack of layers at normal incidence is considered [125, 126]. By resorting to the solution of 1D Maxwell's equations, the electric and magnetic fields component along the incident light direction can be related via the transfer matrix.

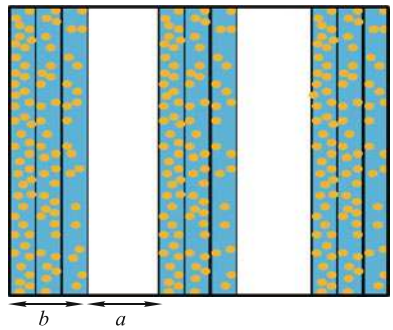

Fig. 13 Schematic structure of 1D GSPCs is shown. It consists of the composite layer and the air layer. The width of the air layer and the composite is a and b respectively. In the composite layer, three layers with different volume fraction are illustrated. Reproduced from Ref. [40].

As metallic nanoparticles are included in the composite film, the local electric field enhancement induced by the third order nonlinearity has to be considered. With Ref. [92] the local electric field inside the nanopartical can be written as $\epsilon_1' = \epsilon_{\mathrm{Ag}} + \epsilon_k \chi^{(3)}$, where $\chi^{(3)}$ is the third order nonlinearity, ϵ_k is equal to $9|\epsilon_{\mathrm{TiO_2}}|/|(2+p)\epsilon_{\mathrm{TiO_2}} + (1-p)\epsilon_{\mathrm{Ag}}|E_0$ and E_0 is the external electric field. The effective dielectric constant of the composite layer (ϵ_e) can be given through the Maxwell–Garnett theory [55]:

$$\frac{\epsilon_e - \epsilon_{\mathrm{TiO_2}}}{\epsilon_e + 2\epsilon_{\mathrm{TiO_2}}} = p\frac{\epsilon_1' - \epsilon_{\mathrm{TiO_2}}}{\epsilon_1' + 2\epsilon_{\mathrm{TiO_2}}} \tag{30}$$

where p is the volume fraction of the nanoparticles in

the composite suspension. ϵ_1' is the dielectric constant of the nanoparticles. ϵ_{TiO_2} is the dielectric constant of TiO_2 and it is fixed as $2.4\epsilon_0$. ϵ_1' is taken as $-9.564\epsilon_0$ for Ag nanoparticles, which is characterized by using the incident wavelength $\lambda = 497$ nm [79].

5.2 Numerical results and discussions

In this section, we present our numerical results (Figs. 14–19) of 1D GSPCs consisting of alternating air layers and Ag nanoparticle based composite layers. With the incorporation of metallic nanoparticles, local electric field induced by the external stimuli has to be included. Let x represent $\chi^{(3)}E_0$. The refraction index of the composite layers as a function of the external electric field stimuli x is illustrated in Fig. 14. It shows that tunable refraction contrast can be obtained when x is changing from 0.0 to 1.0, indicating an enhanced magnitude of external field. With a different magnitude of the external field, the refraction index can be effectively tuned, such spatial modulation opens up a forbidden gap in the electromagnetic dispersion relation.

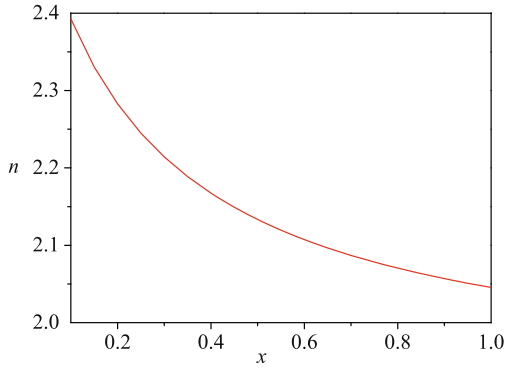

Fig. 14 Refraction index of the composite layer n as a function of the magnitude of the external electric field x is shown. Parameters: $p = 0.15$. Reproduced from Ref. [40].

Figure 15 shows the dispersion relation of the 1D GPCs with different number of composite layer N (2, 5, 10). For the graded profile with 2 layers, $x = 0.1, 0.6$; 5 layers, $x = 0.1, 0.3, 0.5, 0.7, 0.9$; 10 layers, $x = 0.1, 0.2, 0.3, 0.4, 0.5, 0.6, 0.7, 0.8, 0.9, 1.0$. In each composite layer, the volume fraction of the nanoparticles is fixed as $p = 0.15$. Eq. (29) indicates that the composite layer with different number of layers will result in a change of the refraction index in each layer. From Fig. 15, we can find that the photonic band gap is moving towards the low frequency region when the number of layer N is closing to 10. And the photonic band width is getting wider with smaller $N = 2$. Thus, the band gap position and band gap width can be effectively tuned by changing N.

The same as Fig. 15, but in each composite layer, the volume fraction of the nanoparticles are different and the results are shown in Fig. 16. For the graded profile with 2 layers, $p = 0.1, 0.6$; 5 layers, $p = 0.1, 0.3, 0.5, 0.7, 0.9$; 10 layers, $p = 0.1, 0.2, 0.3, 0.4, 0.5, 0.6, 0.7, 0.8, 0.9, 1.0$. With Eq. (30), our results indicate that spectral position of the band gap can effectively be tuned by changing the volume fraction in each composite layer.

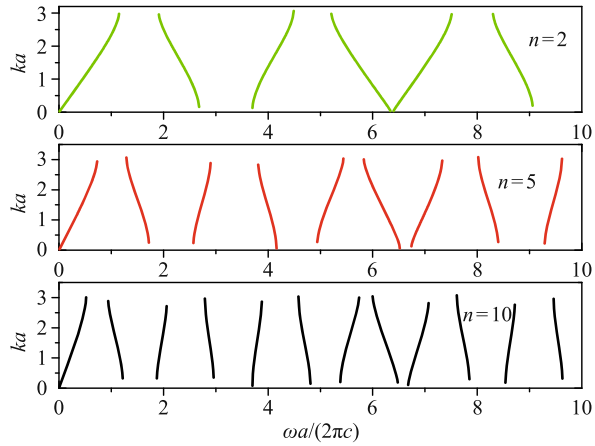

Fig. 15 The dispersion relation in graded multilayer structure with different N is illustrated, where the composite layer has 2, 5, 10 layers respectively. Parameters: $p = 0.15$. (2 layers, $x = 0.1, 0.6$; 5 layers, $x = 0.1, 0.3, 0.5, 0.7, 0.9$; 10 layers, $x = 0.1, 0.2, 0.3, 0.4, 0.5, 0.6, 0.7, 0.8, 0.9, 1.0$). Reproduced from Ref. [40].

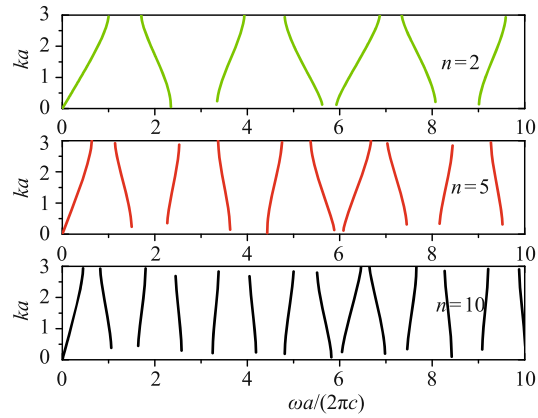

Fig. 16 The dispersion relation in graded multilayer structure with different p is illustrated, where the composite layer has 2, 5, 10 layers respectively. Parameters: $x = 0.1$. (2 layers, $p = 0.1, 0.6$; 5 layers, $p = 0.1, 0.3, 0.5, 0.7, 0.9$; 10 layers, $p = 0.1, 0.2, 0.3, 0.4, 0.5, 0.6, 0.7, 0.8, 0.9, 1.0$). Reproduced from Ref. [40].

In Fig. 15 and Fig. 16, the graded profile (continuous variation in the magnitude of x or p) is investigated. Now we focus on the linear profile, namely, the multilayer structure of PCs is purely constituted by the air layer and composite layer with a fixed x or p. Fig. 17(a) shows that the band gap position is moving towards the high frequency region with an enhanced magnitude of x. But the band gap width is a constant even with different x as shown in Fig. 17(b), which is quite different from that of graded profile (Fig. 15). With a variation of volume fraction p in the composite layer, the results

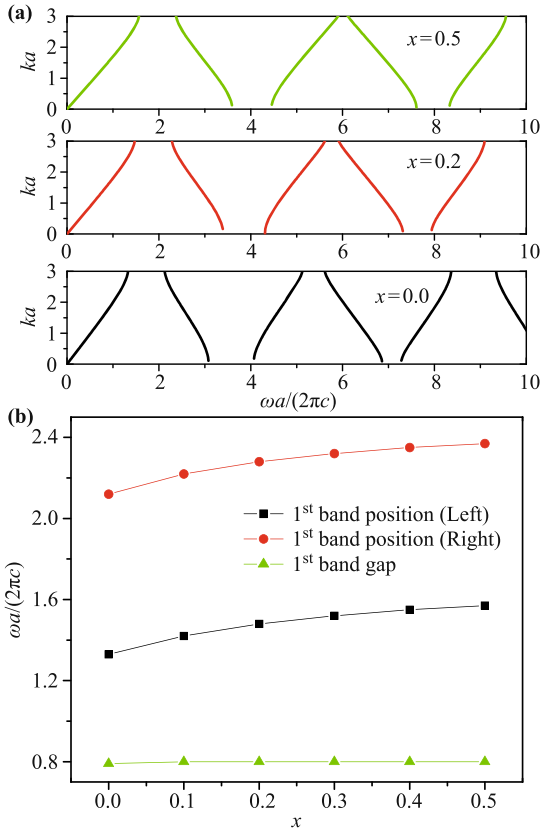

Fig. 17 The dispersion relation in multilayer structure with different external stimuli ($x = 0.0$, $x = 0.2$, $x = 0.5$) is shown in **(a)**. The position and width of the first band gap in the multilayer structure as a function of the applied field x is shown in **(b)**. Parameters: $p = 0.15$, $a = 0.5$, $b = 0.5$. Reproduced from Ref. [40].

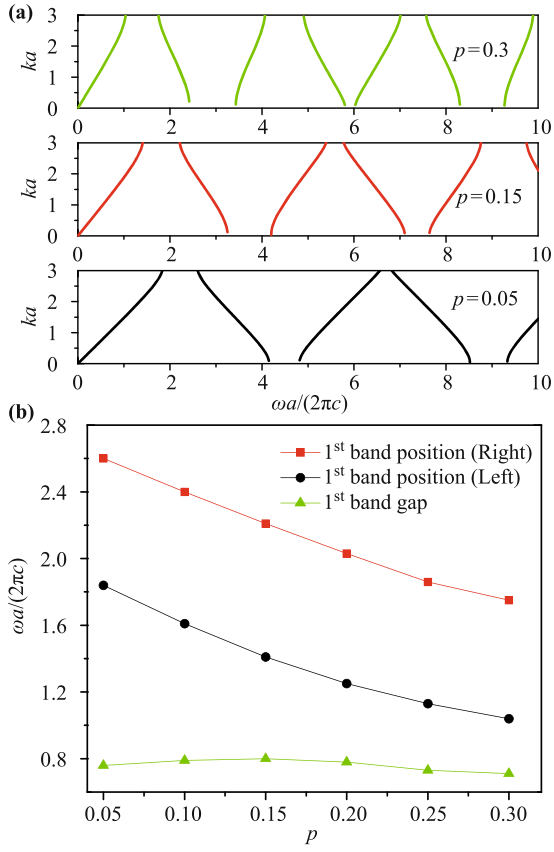

Fig. 18 The dispersion relation in multilayer structure with different volume fraction of the nanoparticle ($p = 0.05$, $p = 0.15$, $p = 0.3$) is shown in **(a)**. The position and width of the first band gap in the multilayer structure as a function of the volume fraction p is shown in **(b)**. Parameters: $x = 0.1$, $a = 0.5$, $b = 0.5$. Reproduced from Ref. [40].

are shown in Fig. 18. With a low volume fraction, the photonic band gap position [Fig. 18(a)] moves towards the low frequency region. The first band widths are also calculated in Fig. 18(b) in green curve. It is found that the band gap width is still invariant in the linear profile even with different p.

In Fig. 19(a), the dispersion relation with linear profile through the variation of the corresponding thickness of the two alternating layers is explored. Here we keep the lattice constant d as a constant. When the thickness of the composite layer d_2 is taken from 0.5, 0.7 to 0.9, the band gap position will move towards the high frequency region. Meanwhile, the first band gap width is getting larger with an increased d_2, as shown in Fig. 19(b).

As we know, PCs are designed to affect the propagation properties of photons. The periodic spatial modulation opens up a forbidden gap in the electromagnetic dispersion relation. In our proposed 1D GSPCs, the refraction index can be effectively tuned by the external electric field, the volume fraction of the nanoparticles and the number of graded composite layer.

6 Second-harmonic generation with magnetocontrolling abilities in ferrofluids

In this part, the nonlinear photonic responses of soft materials based on ferrofluids are presented [41]. We first introduce second harmonic crystals with magnetocontrolling abilities about the proposed soft material. Theoretical [127] and experimental [128–130] reports suggested that spherical particles exhibit a rather unexpected and nontrivial behavior, second harmonic generation (SHG), due to the broken inversion symmetry at particle surfaces, despite their central symmetry which seemingly prohibits second-order nonlinear effects. In colloidal suspensions, the SHG response for centrosymmetric particles was experimentally reported [128]. Most recently, the SHG from centrosymmetrical structure has received extensive attention (e.g., see Refs. [131–133]). In view of recent advancements in the fabrication of nanoshells [134, 135] and single domain ferromagnetic nanoparticles [136], we shall theoretically suggest a class of nonlinear optical materials in which single domain ferromagnetic nanoparticles coated by a nonmagnetic nanoshell with

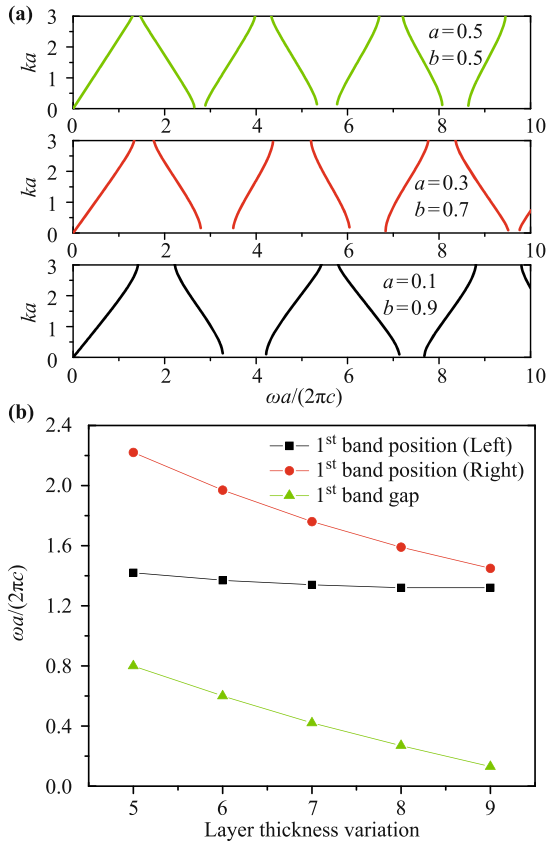

Fig. 19 The dispersion relation in multilayer structure with different thickness in the composite layer is shown in **(a)**. Parameters: $a = 0.5$, $b = 0.5$; $a = 0.3$, $b = 0.7$; $a = 0.1$, $b = 0.9$. The position and width of the first band gap as a function of the thickness in the multilayer structure is shown in **(b)**. Parameters: $x = 0.1$, $p = 0.15$. Reproduced from Ref. [40].

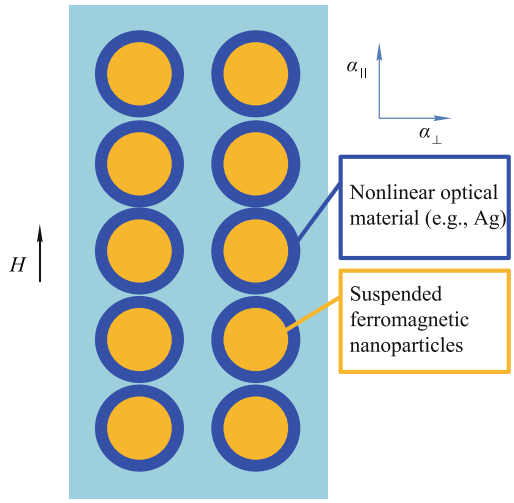

Fig. 20 Design for a nonlinear optical material, which is subjected to an external magnetic field H. $\parallel$ (or $\perp$): Longitudinal (or perpendicular) field cases corresponding to the fact that the E field of an incident light is parallel or perpendicular to the nanoparticle chain. Reproduced from Ref. [41].

an intrinsic SHG susceptibility are suspended in a nonmagnetic host fluid (Fig. 20). For such a material, there is not only an incident light, but also an external magnetic field $\boldsymbol{H}$. The latter yields the formation of chains of coated and thus yields the effective SHG with magnetic-field controllabilities [137–139]. This kind of SHG is expected to receive a broad interest in the physics, optics, and engineering communities, because it is difficult or impossible to achieve conventional, naturally occurring materials or random composites [55, 106, 140–143].

6.1 Formulism

When a collection of objects (e.g., coated nanoparticles or nanoparticle chains) whose size and spacing are much smaller than the wavelength λ of an incident light, the light passing through the structure cannot tell the difference, and hence the inhomogeneous structure can be seen as a homogeneous one [144]. In this regard, to investigate the SHG responses of the proposed material, we are allowed to average over inhomogeneous coated nanoparticles or nanoparticle chains, conceptually replacing the inhomogeneous objects by a homogeneous material (Figs. 21 and 22).

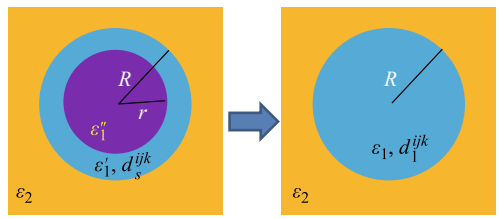

Fig. 21 Schematic graph showing the equivalence between a coated inhomogeneous nanoparticle (left) and a homogeneous nanoparticle (right). Reproduced from Ref. [41].

Let us consider a linear ferromagnetic spherical nanoparticle with dielectric constant ϵ_1'' and radius r, which is coated by a nonlinear optical nonmagnetic nanoshell (e.g., noble metals like silver or gold) with frequency-dependent dielectric constant $\epsilon_1'(\omega)$ and intrinsic SHG susceptibility $d_s^{ijk}(-2\omega;\omega,\omega)$ with each of the superscripts running over the three Cartesian indices. Here ω denotes the angular frequency of a monochromatic external electric field, and the radius of the whole coated nanoparticle is represented as R in the following. All the coated nanoparticles are suspended in a linear nonmagnetic host fluid of ϵ_2. In the nanoshell, the local constitutive relation between the displacement field $\boldsymbol{D}_s$ and the electric field $\boldsymbol{E}_s$ in the static case is given by

$$D_s^i = \sum_j \epsilon_1'(\omega)^{ij} E_s^j + \sum_{jk} d_s^{ijk}(-2\omega;\omega,\omega) E_s^j E_s^k \quad (i = x, y, z) \tag{31}$$

where D_s^i and E_s^i are the ith component of $\boldsymbol{D}_s$ and $\boldsymbol{E}_s$, respectively. Here $\epsilon_1'(\omega)^{ij} = \epsilon_1'(\omega)\delta_{ij}$ denotes the linear dielectric constant, which is assumed for simplicity to be isotropic. Upon certain symmetry, one can have

$$d_s^{iii}(-2\omega;\omega,\omega) \neq 0 (i=x,y,z) \tag{32}$$

$$d_s^{xxx}(-2\omega;\omega,\omega) = d_s^{yyy}(-2\omega;\omega,\omega) = d_s^{zzz}(-2\omega;\omega,\omega) \tag{33}$$

If a monochromatic external field is applied, the nonlinearity in the system will generally generate local potentials and fields at all harmonic frequencies. For a finite-frequency external electric field of the form $E_0 = E_0(\omega)\mathrm{e}^{-\mathrm{i}\omega t} + c.c.$, the equivalent and effective SHG susceptibilities for the coated nanoparticle and the whole suspension, $d_1^{zzz}(-2\omega;\omega,\omega)$ [Eq. (35)] and $d_e^{zzz}(-2\omega;\omega,\omega)$ [Eq. (40)], can be Reproduced by considering the volume average of the displacement field at the frequency 2ω in the inhomogeneous medium. The electric field $\boldsymbol{E}_s$ in the nanoshell can be calculated [140] using standard electrostatics, by solving the corresponding Maxwell equation $\nabla \times \boldsymbol{E}_s = 0$, which implies that $\boldsymbol{E}_s = -\nabla\phi$, where ϕ is an electric potential. Next, the equivalent linear dielectric constant $\epsilon_1(\omega)$ for the coated nanoparticle can be given by the Maxwell–Garnett formula [106]:

$$\frac{\epsilon_1(\omega)-\epsilon_1'(\omega)}{\epsilon_1(\omega)+2\epsilon_1'(\omega)} = (1-f)\frac{\epsilon_1''-\epsilon_1'(\omega)}{\epsilon_1''+2\epsilon_1'(\omega)} \tag{34}$$

where $f = 1-r^3/R^3$ is the volume ratio of the nanoshell to the whole coated nanoparticle. The Maxwell-Garnett formula is a well-known asymmetrical effective medium theory, and may thus be valid for a low concentration of nanoparticles in composites [107]. While treating a single coated nanoparticle with full range $0 \leqslant f \leqslant 1$, the Maxwell–Garnett formula [Eq. (34)] holds for the calculation of $\epsilon_1(\omega)$ indeed due to the natural existence of asymmetry in the coated nanoparticle. The solution of $\boldsymbol{E}_s$ in Ref. [140] can be used to derive the equivalent SHG susceptibility for the coated nanoparticle, $d_1^{iii}(-2\omega;\omega,\omega)$, which can be expressed as

$$d_1^{iii}(-2\omega;\omega,\omega) = f d_s^{iii}(-2\omega;\omega,\omega) \times \sum_{j=x}^{z}\langle\frac{E_{s,j}(2\omega)}{E_{0,i}(2\omega)}\left(\frac{E_{s,j}(\omega)}{E_{0,i}(\omega)}\right)^2\rangle_s \tag{35}$$

where $\langle\cdots\rangle_s$ denotes a volume average over the nanoshell. To show the feature of the proposed material, we assume the optical responses [namely, $\epsilon_1(\omega)$ and $d_1^{iii}(-2\omega;\omega,\omega)$] of an equivalent spheroid or a chain (see Fig. 21) to be the same as those of each coated nanoparticle inside the spheroid or chain. For convenience, the suspension is further assumed to be the one that contains identical equivalent spheroids with geometrical depolarization factor $\alpha_\parallel$ (or $\alpha_\perp$) along major (or minor) axis (Fig. 22). In the following, α is also called *local magnetic field factors*, because, from the physical point of view, the spheroids (or chains) are just formed due to the application of external magnetic fields. In this connection, the summation term in Eq. (35) admits $\{\Pi(2\omega)\Pi^2(\omega) + (4/5)(rR)^{-3}[\Pi(2\omega)p_s^2(\omega) + 2\Pi(\omega)p_s(2\omega)p_s(\omega)] + (8/35)(r^3+R^3)/(r^6R^6)p_s(2\omega)p_s^2(\omega)\}/[E_{0,i}(2\omega)E_{0,i}^2(\omega)]$ where

$$\Pi(\omega) = T_s(\omega)E_{0,i}(\omega)$$
$$p_s(\omega) = b_s(\omega)r^3T_s(\omega)E_{0,i}(\omega) \tag{36}$$

with

$$b_s(\omega) = (\epsilon_1''-\epsilon_1'(\omega))/(\epsilon_1''+2\epsilon_1'(\omega)) \tag{37}$$

and $T_s(\omega) = [\Theta(\omega) + 2b_s(\omega)(\Theta(\omega)-1)(1-f)]^{-1}$. Here $\Theta(\omega) = [\epsilon_1'(\omega)+2\epsilon_2]/(3\epsilon_2)$.

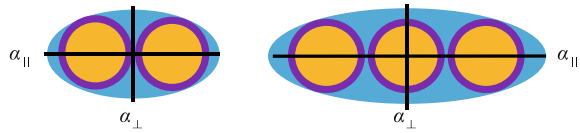

Fig. 22 Schematic graph showing the equivalence between nanoparticle chains and spheroids with geometrical major-axis (or minoraxis) depolarization factor $\alpha_\parallel$ (or $\alpha_\perp$). The major axis is parallel to external magnetic fields. α is also called local magnetic field factors. Reproduced from Ref. [41].

In the following analysis, we assume the spheroidal particle possess the same linear response as the coated particle. But, for the nonlinear response, to include the shape effect, let us introduce a local magnetic field factor α that denotes $\alpha_\parallel$ and $\alpha_\perp$ for longitudinal and transverse field cases, respectively (Figs. 21 and 22). There is a sum rule for $\alpha_\parallel$ and $\alpha_\perp$, $\alpha_\parallel + 2\alpha_\perp = 1$ [145]. The parameter α measures the degree of structural anisotropy due to the formation of nanoparticle chains, which is induced to appear by the external magnetic field $\boldsymbol{H}$. More precisely, the degree of the magnetic-field-induced anisotropy is measured by how much α deviates from $1/3$, $1/3 < \alpha_\perp < 1$ and $0 < \alpha_\parallel < 1/3$. As H increases, $\alpha_\perp$ and $\alpha_\parallel$ should tend to 1 and 0, respectively, which is indicative of the formation of longer nanoparticle chains (or equivalent spheroids). Therefore, α should be a function of external magnetic fields H. Specifically, for $H = 0$ there is $\alpha_\parallel = \alpha_\perp = 1/3$, which corresponds to an isotropic system in which all the coated nanoparticles are randomly distributed in the suspension. After the introduction of α, while we assume the spheroid possess the same nonlinear response as the coated particle, for more accurate estimation of the nonlinear response of the spheroid, let us replace $\Theta(\omega) = [\epsilon_1'(\omega)+2\epsilon_2]/(3\epsilon_2)$ with $\Theta(\omega) = [\epsilon_2 + \alpha(\epsilon_1'(\omega)-\epsilon_2)]/\epsilon_2$. That is, the shape effect of spheroids has been included. Apparently, the substitution of $\alpha = 1/3$ into Eq. (35) yields the same expression as Eq. (15) in Ref. [140] in which a random composite of particles with nonlinear non-metallic shells was investigated. Alternatively, according to the calculation of major-axis depolarization factor L of prolate

spheroids [145]:

$$L = 1/(1-\rho^2) + \rho/(\rho^2-1)^{3/2}\ln(\rho+\sqrt{\rho^2-1}) \quad (38)$$

where $\rho(>1)$ is the ratio between the major and minor axes of the elliptic cross section, α can be given in terms of the number n of nanoparticles in an equivalent spheroid (or a chain):

$$\alpha_{\|} = \frac{1}{1-n^2} + \frac{n}{(n^2-1)^{3/2}}\ln(n+\sqrt{n^2-1}) \quad (39)$$

Throughout this section, both the nano-shell and host fluid are nonmagnetic, and the core is ferromagnetic. The existence of ferromagnetism in the core makes the chain formation possible as long as an external magnetic field H is applied [137]. We have added the magnetic contribution to the expressions for optical responses through the local magnetic field factor α. So far the exact relation between α and H lacks because it relates to complicated suspension hydrodynamics and kinetics at nonequilibrium. Nevertheless, the results obtained from Fig. 23 are valid for equilibrium systems in which neither hydrodynamics nor kinetics can affect the SHG. Without loss of any generality, to capture the features and their physics of the proposed materials, we use α to represent the strength of the external magnetic field H in Fig. 23.

Now we see the suspension as the one in which the equivalent spheroids with $\epsilon_1(\omega)$ [Eq. (34)] and $d_1^{iii}(2\omega;\omega,\omega)$ [Eq. (35)] are embedded in the host fluid. Owing to the $z-$directed external magnetic field, all the spheroids should also be directed along z axis, but with the locations being randomly distributed. According to the general expression for the effective SHG susceptibility [140], we take one step forward to express the effective SHG susceptibility $d_e^{iii}(-2\omega;\omega,\omega)$ for the whole suspension in the dilute limit:

$$d_e^{iii}(-2\omega;\omega,\omega) = p d_1^{iii}(-2\omega;\omega,\omega)\Gamma(2\omega)\Gamma^2(\omega) \quad (40)$$

where p is the volume fraction of the coated nanoparticles. In Eq. (40), $\Gamma(\omega)$ is a local electric field enhancement factor, and it is obtained by deriving the factor in a spheroid of depolarization factor α with principle axes along external electric fields, $\Gamma(\omega) = \epsilon_2/[\epsilon_2 + \alpha(\epsilon_1(\omega) - \epsilon_2)]$.

Since metal surfaces were used to obtain enhanced SHG responses [146], for our numerical simulations we take a Drude dielectric function (that is valid for noble metals within the frequency range of interest) for $\epsilon_1'(\omega)$:

$$\epsilon_1'(\omega) = \epsilon(\infty) - (\epsilon(0)-\epsilon(\infty))\omega_p^2/[\omega(\omega+\mathrm{i}\gamma)] \quad (41)$$

where ω_p is the bulk plasmon frequency (which is proportional to the surface plasmon frequency ω_{sp}, e.g., $\omega_p = \sqrt{3}\omega_{sp}$ for a sphere [147],) $\epsilon(\infty)$ the high-frequency limit dielectric constant, $\epsilon(0)$ the static dielectric constant, and γ the collision frequency. Specifically, for silver, $\epsilon(\infty) = 5.45$, $\epsilon(0) = 6.18$, and $\omega_p = 1.72\times10^{16}$ rad/s [105]. In addition, we take $\gamma = 0.01\omega_p$ (a typical value for metals), $r = 5$ nm (a typical value for single domain ferromagnetic nanoparticles [137],) the thickness of nanoshells 1.9 nm (or $R = 6.9$ nm), $\epsilon_1'' = -25 + 4i$ (e.g., for cobalt), frequency-independent dielectric constant $\epsilon_2 = 1.77$ (high-frequency limit dielectric constant of water), and $p = 0.18$. Based on the values of r, R and p, we obtain the volume fractions, p_c and p_s, of the ferromagnetic and nonlinear optical components in the whole suspension, $p_c = 0.07$ and $p_s = 0.11$, according to the relations $R/r = (1+p_s/p_c)^{1/3}$ and $p = p_c + p_s$. We shall investigate the light energy 1–5 eV, which corresponds to the wavelength $\lambda = 248$–1242 nm, or the frequency range $\omega = 1.52\times10^{15}$–$7.59\times10^{15}$ rad/s.

6.2 Numerical results and discussions

We show the effective SHG susceptibility $d_e^{iii}(-2\omega;\omega,\omega)$ of the whole suspensions in Fig. 23. For longitudinal field cases [Fig. 23(a), (b), (f), and (g)], as $\alpha_{\|}$ decreases (i.e., external applied magnetic field H increases, and longer nanoparticle chains are formed accordingly), the resonant peak in the SHG response is not only red-shifted (namely, located at a lower frequency), but also further enhanced, when compared to the isotropic case at zero external magnetic field $H = 0$ [Fig. 23(c) and (h)]. However, inverse behavior appears for transverse field cases [Fig. 23(d), (e), (i), and (j)]. In detail, for transverse field cases, as the external magnetic field increases, the resonant peak in the SHG signal is both reduced and blue-shifted (i.e., located at higher frequency), and hence becomes less attractive.

When the magnetic field is applied, the coated nanoparticles will form chains, thus changing the microstructure of the system accordingly. For longitudinal field cases, the nonlinear component will become more abundant along the chains than perpendicular to the chains for transverse field. When there is an incident light, the nonlinear component in the system will generally generate local potentials and fields at all harmonic frequencies. The formation of nanoparticle chains due to the application of external magnetic fields changes the surrounding circumstance of each coated nanoparticle naturally, which in turn affects the local electric field in the nanoshells and hence shifts the resonant plasmon frequency at which the resonant peak appears (Fig. 23). Therefore, in the presence of an external magnetic field, the SHG response becomes anisotropic (i.e., its strength in the longitudinal field differs from that in the transverse field), and the degree of anisotropy can further be adjusted by tuning the external magnetic field. That is,

the SHG response of the system can be affected accordingly. In looking for experimental evidence, we note that Du and Luo have reported nonlinear optical effects in suspensions of ferromagnetic nanoparticles (with mean diameter 9 nm) in kerosene [148]. They have observed that the nonlinear optical effect is enhanced by applying a moderate magnetic field. However, this mechanism was unclear at that time. Based on the present section, it seems that this enhanced nonlinear optical effect results from the magnetic field-induced anisotropic structure.

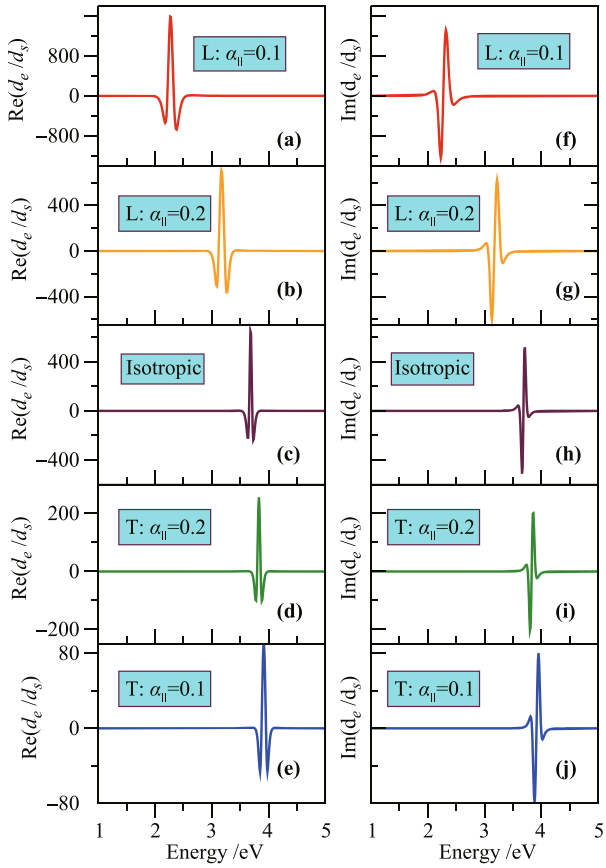

Fig. 23 [**(a)**–**(e)**] Real and [**(f)**–**(j)**] imaginary parts of the effective SHG susceptibility $d_e^{iii}(-2\omega;\omega,\omega) \equiv d_e$ normalized by the intrinsic SHG susceptibility in the nonlinear nanoshell $d_s^{iii}(-2\omega;\omega,\omega) \equiv d_s$ for different external magnetic fields represented by local magnetic field factors vs the energy of an incident light. Here L and T denote the longitudinal and transverse field cases, respectively. According to Eq. (38), the number n of nanoparticles in the chains is $n \approx 3$ for $\alpha_{\|} = 0.1$ and $n \approx 2$ for $\alpha_{\|} = 0.2$. Note in (d), (e), (i) and (j) the corresponding $\alpha_{\perp}$ in use can be calculated according to the relation $\alpha_{\|} + 2\alpha_{\perp} = 1$. Reproduced from Ref. [41].

7 Conclusions

We have reviewed the optical properties of magnetic-field controllable 1D SPCs. The proposed structure is constituted by alternating ferrofluid layers and dielectric layers. Due to the magnetic field response of the ferromagnetic nanoparticles, they can align along the external field direction, thus changing the microstructure of the system correspondingly. In 1D SPCs, the photonic band gap can be effectively tuned with the initiation of an external magnetic field and the volume fraction of the nanoparticles. For the ferromagnetic nanoparticles coated with metallic layer in ferrofluids, the absorption effect in the 1D SPCs has to be included. The solution of the complex transfer matrix method, indicates that an additional band gap appears in the lower frequency region. And these band gaps blueshift when the external magnetic field is enhanced, and redshift when the thickness of metallic layer is increased. Graded multilayer in the SPCs is studied through a varying number of deposited ferrofluid layers. By regarding each layer in the multilayer structure as a series of capacitance, the effective dielectric constant is derived. Our results show that the position and width of the photonic band gap can be effectively modulated by varying the number of graded composite layer, the volume fraction of nanoparticles and the external stimuli. Finally, the nonlinear optical response (namely, SHG) in ferrofluids has been introduced, and the numerical results show that such materials possess magnetic-field controllabilities, redshift, and enhancement. The utilization of magnetic field in nanoscale assembly is of both fundamental and practical interests. It not only helps to probe colloidal interactions, but also allows the creation of novel complex structures and the fabrication of advanced photonic devices.

Acknowledgements C. Z. Fan and E. J. Liang acknowledge the financial support by the National Natural Science Foundation of China (Grant No. 11104252), the Ministry of Education of China (No. 20114101110003), by the fund for Science and Technology innovation team of Zhengzhou (2011-03), the Basic and Frontier Technology Research Program of Henan Province (No. 122300410162), and the cooperation fund with Fudan University (No. KL2011-01). J. P. Huang acknowledges the support by the Chinese National Key Basic Research Special Fund under Grant No. 2011CB922004, Fok Ying Tung Education Foundation under Grant No. 131008, the National Natural Science Foundation of China under Grant Nos. 11075035 and 11222544, and Shanghai Rising-Star Program (No. 12QA1400200).

References

1. N. Masaya, Rep. Prog. Phys., 2010, 73: 096501
2. J. D. Joannopoulos, S. G. Johnson, J. N. Winn, and R. D. Meade, Photonic Crystals: Molding the Flow of Light, 2nd Ed., Princeton: Princeton University Press, 2008
3. E. Yablonovitch, Phys. Rev. Lett., 1987, 58(20): 2059
4. S. John, Phys. Rev. Lett., 1987, 58(23): 2486
5. Y. Zhang, J. Wang, Y. Huang, Y. Song, and L. Jiang, J. Mater. Chem., 2011, 21(37): 14113

6. Q. Y. Zhu, Y. Q. Fu, D. Q. Hu, and Z. M. Zhang, Chin. Phys. B, 2012, 21(6): 064220
7. J. Wang, M. Yan, and M. Qiu, Front. Phys. China, 2010, 3(3): 260
8. P. E. Barclay, K. Srinivasan, and O. Painter, Opt. Express, 2005, 13(3): 801
9. M. Lonččar, T. Doll, J. Vučković, and A. Scherer, J. Lightwave Tech., 2000, 18: 1402
10. T. Zijlstra, E. van der Drifta, M. J. A. de Dood, E. Snoeks, and A. Polman, J. Vac. Sci. Technol. B, 1999, 17(6): 2734
11. S. H. Kim, S. Y. Lee, S. M. Yang, and G. R. Yi, NPG Asia Mater., 2011, 3(1): 25
12. P. Jiang, J. M. Smith, J. M. Ballato, and S. H. Foulger, Adv. Mater., 2005, 17(2): 179
13. Y. J. Zhao, Z. Y. Xie, H. C. Gu, L. Jin, X. W. Zhao, B. P. Wang, and Z. Z. Gu, NPG Asia Mater., 2012, 4(9): e25
14. M. Honda, T. Seki, and Y. Takeoka, Adv. Mater., 2009, 21(18): 1801
15. V. V. Ravi Kanth Kumar, A. K. George, W. H. Reeves, J. C. Knight, P. S. J. Russell, F. G. Omenetto, and A. J. Taylor, Opt. Express, 2002, 10: 1520
16. J. D. Debord, S. Eustis, S. B. Debord, M. T. Lofye, and L. A. Lyon, Adv. Mater., 2002, 14(9): 658
17. R. E. Rosensweig, Ferrohydrodynamics, New York: Cambridge University Press, 1985
18. Y. H. Ye, T. S. Mayer, I. C. Khoo, I. B. Divliansky, N. Abrams, and T. E. Mallouk, J. Mater. Chem., 2002, 12(12): 3637
19. L. He, Y. X. Hu, X. G. Han, Y. Lu, Z. D. Lu, and Y. D. Yin, Langmuir, 2011, 27(22): 13444
20. W. Cheng, K. B. Tang, and J. Sheng, Chem. -Eur. J., 2010, 16(12): 3608
21. X. L. Xu, G. Friedman, K. D. Humfeld, S. A. Majetich, and S. A. Asher, Chem. Mater., 2002, 14(3): 1249
22. X. L. Xu, G. Friedman, K. D. Humfeld, S. A. Majetich, and S. A. Asher, Adv. Mater., 2001, 13(22): 1681
23. N. Yanase, H. Noguchi, H. Asakura, and T. Suzuta, J. Appl. Polym. Sci., 1993, 50(5): 765
24. Y. X. Hu, L. He, and Y. D. Yin, Angew. Chem. Int. Ed., 2011, 50(16): 3747
25. J. P. Ge, Y. X. Hu, and Y. D. Yin, Angew. Chem., 2007, 119(39): 7572
26. L. He, Y. X. Hu, H. Kim, J. P. Ge, S. Kwon, and Y. D. Yin, Nano Lett., 2010, 10(11): 4708
27. P. C. Morais, V. K. Garg, A. C. Oliveira, L. P. Silva, R. B. Azevedo, A. M. L. Silva, and E. C. D. Lima, J. Magn. Magn. Mater., 2001, 225(1–2): 37
28. A. F. Bakuzis, K. Skeff Neto, P. P. Gravina, L. C. Figueiredo, P. C. Morais, L. P. Silva, R. B. Azevedo, and O. Silva, Appl. Phys. Lett., 2004, 84(13): 2355
29. T. A. Eloim, P. C. Santos, Morais, and A. F. Bakuzis, Phys. Rev. E, 2010, 82: 21407
30. C. Scherer and A. M. Figueiredo Neto, Braz. J. Phys., 2005, 35(3a): 718
31. Y. Gao, J. P. Huang, Y. M. Liu, L. Gao, K. W. Yu, and X. Zhang, Phys. Rev. Lett., 2010, 104(3): 034501
32. X. D. Zhang, Front. Phys. China, 2006, 1(4): 396
33. B. M. Berkovsky, V. F. Medvedev, and M. S. Krakov, Magnetic Fluids: Engeering Applications, New York: Oxford University Press, 1993
34. C. Alexiou, W. Arnold, P. Hulin, R. J. Klein, H. Renz, and F. G. Parak, Magnetohydrodynamics, 2001, 37: 318
35. I. Robinson, D. Tung, S. Maenosono, C. Wälti, and N. T. K. Thanh, Nanoscale, 2010, 2(12): 2624
36. H. Rahn, I. Gomez-Morilla, R. Jurgons, Ch. Alexiou, and S. Odenbach, J. Phys.: Condens. Matter, 2008, 20(20): 204152
37. J. D. A. Gomes, M. H. Sousa, F. A. Tourinho, R. Aquino, G. J. da Silva, J. Depeyrot, E. Dubois, and R. Perzynski, J. Phys. Chem. C, 2008, 112(16): 6220
38. C. Z. Fan, G. Wang, and J. P. Huang, J. Appl. Phys., 2008, 103(9): 094107
39. C. Z. Fan, E. J. Liang, and J. P. Huang, J. Phys. D, 2011, 44(32): 325003
40. C. Z. Fan, J. Q. Wang, J. N. He, P. Ding, and E. J. Liang, Chin. Phys. B, 2012 (accepted)
41. C. Z. Fan and J. P. Huang, Appl. Phys. Lett., 2006, 89(14): 141906
42. Y. Gao, C. Z. Fan, and J. P. Huang, Progress in Physics, 2010, 30: 387
43. D. M. Topasna and G. A. Topasna, Numerical modeling of thin film optical filters, in Education, Training in Optics, 2009, Photonics, OSA Technical Digest Series (CD) Optical Society of America, paper EP5
44. J. D. Jackson, Classical electrodynamics, Berkeley: University of California, 2004
45. C. C. Katsidis and D. I. Siapkas, Appl. Opt., 2002, 41(19): 3978
46. X. Y. Wu, B. J. Zhang, J. H. Yang, X. J. Liu, N. Ba, Y. H. Wu, and Q. C. Wang, Physica E, 2011, 43(9): 1694
47. C. K. Lo and K. W. Yu, Phys. Rev. E, 2001, 64(3 Pt 1): 031501
48. K. Butter, P. H. H. Bomans, P. M. Frederik, G. J. Vroege, and A. P. Philipse, J. Phys.: Condens. Matter, 2003, 15(15): S1451
49. K. Butter, P. H. H. Bomans, P. M. Frederik, G. J. Vroege, and A. P. Philipse, Nat. Mater., 2003, 2(2): 88
50. R. A. Trasca and S. H. L. Klapp, J. Chem. Phys., 2008, 129(8): 084702
51. M. Klokkenburg, B. H. Erné, J. D. Meeldijk, A. Wiedenmann, A. V. Petukhov, R. P. Dullens, and A. P. Philipse, Phys. Rev. Lett., 2006, 97(18): 185702
52. M. Klokkenburg, B. H. Erné, A. Wiedenmann, A. V. Petukhov, and A. P. Philipse, Phys. Rev. E, 2007, 75(5 Pt 1): 051408
53. Z. W. Wang, C. Holm, and H. W. Müller, Phys. Rev. E, 2002, 66(2 Pt 1): 021405
54. J. T. K. Wan, G. Q. Gu, and K. W. Yu, Phys. Rev. E, 2001, 63(5 Pt 1): 052501

55. J. P. Huang and K. W. Yu, Phys. Rep., 2006, 431(3): 87
56. C. Cotae, O. Baltag, R. Olaru, D. Calarasu, and D. Costandache, J. Magn. Magn. Mater., 1999, 201(1-3): 394
57. C. P. Pang, C. T. Hsieh, and J. T. Lue, J. Phys. D, 2003, 36(15): 1764
58. J. P. Huang, Z. W. Wang, and C. Holm, Phys. Rev. E, 2005, 71(6 Pt 1): 061203
59. M. Centini, C. Sibilia, M. Scalora, G. D'Aguanno, M. Bertolotti, M. J. Bloemer, C. M. Bowden, and I. Nefedov, Phys. Rev. E, 1999, 60(4 Pt B): 4891
60. M. Scalora, M. J. Bloemer, A. S. Manka, J. P. Dowling, R. Viswanathan, J. W. Haus, and C. M. Bowden, Phys. Rev. A, 1997, 56(4): 3166
61. J. P. Ge and Y. D. Yin, Angew. Chem. Int. Ed., 2011, 50(7): 1492
62. A. Mekis, J. C. Chen, I. Kurland, S. H. Fan, P. R. Villeneuve, and J. D. Joannopoulos, Phys. Rev. Lett., 1996, 77(18): 3787
63. T. R. Zhai, D. H. Liu, and X. D. Xiang, Front. Phys. China, 2010, 5(3): 266
64. K. Chang, J. T. Liu, J. B. Xia, and N. Dai, Appl. Phys. Lett., 2007, 91(18): 181906
65. G. J. Lee, Y. P. Lee, S. G. Jung, C. K. Hwangbo, S. Kim, and I. Park, J. Appl. Phys., 2007, 102(7): 073528
66. G. Wang, J. P. Huang, and K. W. Yu, Appl. Phys. Lett., 2007, 91(19): 191117
67. M. Golosovsky, Y. Neve-Oz, and D. Davidovm, Synth. Met., 2003, 139(3): 705
68. J. P. Ge, Y. X. Hu, and Y. D. Yin, Angew. Chem. Int. Ed., 2007, 46(39): 7428
69. S. Kim and V. Gapalan, Appl. Phys. Lett., 2001, 78(20): 3015
70. J. M. Weissman, H. B. Sunkara, A. S. Tse, and S. A. Asher, Science, 1996, 274(5289): 959
71. D. McPhail, M. Straub, and M. Gu, Appl. Phys. Lett., 2005, 87(9): 091117
72. K. Busch and S. John, Phys. Rev. Lett., 1999, 83(5): 967
73. E. Graugnard, D. P. Gaillot, S. N. Dunham, C. W. Neff, T. Yamashita, and C. J. Summers, Appl. Phys. Lett., 2006, 89(18): 181108
74. P. Kopperschmidt, Appl. Phys. B, 2001, 73(7): 717
75. D. McPhail, M. Straub, and M. Gu, Appl. Phys. Lett., 2005, 86(5): 051103
76. C. K. Lo and K. W. Yu, Phys. Rev. E, 2001, 64(3 Pt 1): 031501
77. C. K. Lo, J. T. K. Wan, and K. W. Yu, J. Phys.: Condens. Matter, 2001, 13(6): 1315
78. J. P. Huang, J. T. K. Wan, C. K. Lo, and K. W. Yu, Phys. Rev. E, 2001, 64(6 Pt 1): 061505
79. P. B. Johnson and R. W. Christy, Phys. Rev. B, 1974, 9(12): 5056
80. J. Zi, J. Wan and C. Zhang, Appl. Phys. Lett., 1998, 73(15): 2084
81. R. R. Kellner and W. Koehler, J. Appl. Phys., 2005, 97(3): 034910
82. J. D. Joannopoulos, P. R. Villeneuve, and S. Fan, Nature, 1997, 386(6621): 143
83. Y. A. Vlasov, X. Z. Bo, J. C. Sturm, and D. J. Norris, Nature, 2001, 414(6861): 289
84. M. Fu, J. Zhou, and J. H. Yu, J. Phys. Chem. C, 2010, 114(20): 9216
85. S. G. Johnson and J. D. Joannopoulos, Opt. Express, 2001, 8(3): 173
86. P. Yeh, Optical Waves in Layered Media, New York: Wiley, 1988
87. M. Lonca, D. Nedeljkovie, T. Doll, J. Vuckovic, A. Schere, and T. P. Pearsall, Appl. Phys. Lett., 2000, 77: 1937
88. M. Campbell, D. N. Sharp, M. T. Harrison, R. G. Denning, and A. J. Turberfield, Nature, 2000, 404(6773): 53
89. C. C. Cheng and A. Scherer, J. Vac. Sci. Technol. B, 1995, 13(6): 2696
90. M. Miyake, Y. C. Chen, P. V. Braun, and P. Wiltzius, Adv. Mater., 2009, 21(29): 3012
91. S. W. Wang, W. Lu, X. S. Chen, Z. F. Li, X. C. Shen, and W. J. Wen, J. Appl. Phys., 2003, 93(11): 9401
92. G. Wang, J. P. Huang, and K. W. Yu, Opt. Lett., 2008, 33(19): 2200
93. J. D. Debord and L. A. Lyon, J. Phys. Chem. B, 2000, 104(27): 6327
94. W. Park and J. B. Lee, Appl. Phys. Lett., 2004, 85(21): 4845
95. X. C. Xu, Y. G. Xi, D. Z. Han, X. H. Liu, J. Zi, and Z. Q. Zhu, Appl. Phys. Lett., 2005, 86(9): 091112
96. D. Soto-Puebla, M. Xiao, and F. Ramos-Mendieta, Phys. Lett. A, 2004, 326(3–4): 273
97. M. Bergmair and K. Hingerl, J. Opt. A, 2007, 9(9): S339
98. C. S. Levin, C. Hofmann, T. A. Ali, A. T. Kelly, E. Morosan, P. Nordlander, K. H. Whitmire, and N. J. Halas, Nano, 2009, 3: 1379
99. S. P. Yeap, P. Y. Toh, A. L. Ahmad, S. C. Low, S. A. Majetich, and J. K. Lim, J. Phys. Chem. C, 2012, 116(42): 22561
100. Y. Song, J. Ding, and Y. H. Wang, J. Phys. Chem. C, 2012, 116(20): 11343
101. Z. C. Xu, Y. L. Hou, and S. H. Sun, J. Am. Chem. Soc., 2007, 129(28): 8698
102. Z. Ban and C. O'Connor, Mat. Res. Soc. Symp. Proc., 2004, 818: M5.18
103. H. Yu, M. Chen, P. M. Rice, S. X. Wang, R. L. White, and S. Sun, Nano Lett., 2005, 5(2): 379
104. V. Kuzmiak and A. A. Maradudin, Phys. Rev. B, 1997, 55(12): 7427
105. P. G. Kik, S. A. Maier, and H. A. Atwater, Phys. Rev. B, 2004, 69(4): 045418
106. R. W. Boyd, Nonlinear Optics, New York: Academic Press, 1992
107. D. J. Bergman and D. Stroud, Solid State Phys., 1992, 46: 147

108. M. Shimomuraa and T. Sawadaishib, Curr. Opin. Colloid Interface Sci., 2001, 6: 11
109. C. Ren, L. F. Cheng, F. Kang, L. Gan, D. Z. Zhang, and Z. Y. Li, Chin. Phys. B, 2012, 21(10): 104210
110. Y. Wang, X. Q. Huang, and C. D. Gong, Chin. Phys. Lett., 2000, 17: 498
111. F. Zhuang, L. Wu, and S. L. He, Chinese Phys., 2002, 11(8): 834
112. L. Li, Y. C. Xie, Y. Q. Wang, X. Y. Hu, Z. F. Feng, and B. Y. Cheng, Chin. Phys. Lett., 2003, 20: 1767
113. V. L. Colvin, MRS Bull., 2001, 26(08): 637
114. S. Colodrero, M. Ocaña, and H. Míguez, Langmuir, 2008, 24(9): 4430
115. S. Colodrero, M. Ocaña, A. R. González-Elipe, and H. Míguez, Langmuir, 2008, 24(16): 9135
116. G. Lozano, S. Colodrero, O. Caulier, M. E. Calvo, and H. Miguez, J. Phys. Chem. C, 2010, 114(8): 3681
117. B. G. Prevo and O. D. Velev, Langmuir, 2004, 20(6): 2099
118. H. Jiang, J. Sabarinathan, T. Manifar, and S. Mittler, J. Lightwave. Tech., 2009, 27: 2264
119. J. Li and Y. Han, Langmuir, 2006, 22(4): 1885
120. S. Suresh, Science, 2001, 292(5526): 2447
121. Q. Su, B. Liu and J. P. Huang, Front. Phys., 2011, 6(1): 65
122. A. B. Shvartsburg, V. Kuzmiak, and G. Petite, Phys. Rep., 2007, 452(2-3): 33
123. H. Rauh, G. I. Yampolskaya, and S. V. Yampolskii, New J. Phys., 2010, 12(7): 073033
124. Z. F. Sang and Z. Y. Li, Opt. Commun., 2007, 273(1): 162
125. L. Shiveshwari and P. Mahto, Solid State Commun., 2006, 138(3): 160
126. X. K. Kong, S. B. Liu, H. F. Zhang, and H. L. Guan, Opt. Commun., 2011, 284(12): 2915
127. J. I. Dadap, J. Shan, K. B. Eisenthal, and T. F. Heinz, Phys. Rev. Lett., 1999, 83(20): 4045
128. N. Yang, W. E. Angerer, and A. G. Yodh, Phys. Rev. Lett., 2001, 87(10): 103902
129. B. Y. Gu and L. M. Zhao, Front. Phys. China, 2007, 2(3): 279
130. J. P. Huang, Front. Phys. China, 2007, 2(1): 17
131. P. Xu, S. H. Ji, S. N. Zhu, X. Q. Yu, J. Sun, H. T. Wang, J. L. He, Y. Y. Zhu, and N. B. Ming, Phys. Rev. Lett., 2004, 93(13): 133904
132. R. Bernal and J. A. Maytorena, Phys. Rev. B, 2004, 70(12): 125420
133. Y. Liu, F. Qin, F. Zhou, Q. B. Meng, D. Z. Zhang, and Z. Y. Li, Front. Phys. China, 2010, 5(3): 220
134. D. B. Mitzi, L. L. Kosbar, C. E. Murray, M. Copel, and A. Afzali, Nature, 2004, 428(6980): 299
135. C. L. Nehl, N. K. Grady, G. P. Goodrich, F. Tam, N. J. Halas, and J. H. Hafner, Nano Lett., 2004, 4(12): 2355
136. V. F. Puntes, P. Gorostiza, D. M. Aruguete, N. G. Bastus, and A. P. Alivisatos, Nat. Mater., 2004, 3(4): 263
137. S. Odenbach, Magnetoviscous Effects in Ferrofluids, Berlin: Springer-Verlag, 2002
138. S. Odenbach and H. Gilly, J. Magn. Magn. Mater., 1996, 152(1–2): 123
139. S. Odenbach and H. Störk, J. Magn. Magn. Mater., 1998, 183(1–2): 188
140. P. M. Hui, C. Xu, and D. Stroud, Phys. Rev. B, 2004, 69(1): 014203
141. J. P. Huang and K. W. Yu, Appl. Phys. Lett., 2004, 85(1): 94
142. J. P. Huang and K. W. Yu, Appl. Phys. Lett., 2005, 86(4): 041905
143. J. P. Huang, Phys. Rev. E, 2004, 70(4 Pt 1): 041403
144. D. R. Smith, J. B. Pendry, and M. C. K. Wiltshire, Science, 2004, 305(5685): 788
145. L. D. Landau, E. M. Lifshitz, and L. P. Pitaevskii, Electrodynamics of Continuous Media, 2nd Ed., New York: Pergamon, 1984
146. M. I. Stockman, D. J. Bergman, C. Anceau, S. Brasselet, and J. Zyss, Phys. Rev. Lett., 2004, 92(5): 057402
147. H. P. Chiang, P. T. Leung, and W. S. Tse, J. Phys. Chem. B, 2000, 104(10): 2348
148. T. Du and W. Luo, Appl. Phys. Lett., 1998, 72(3): 272